Neutral and methylated cationic Re(I) tetrazolato complexes: comparative photophysics, resonance Raman spectroscopy and fabrication of OLED and LEEC devices

Melissa V. Werrett,[a,b] Gregory S. Huff,[c,d] Sara Muzzioli,[b] Valentina Fiorini,[b] Stefano Zacchini,[b] Brian W. Skelton,[e] Antonio Maggiore,[f] Joanna M. Malicka,[f] Massimo Cocchi,[f,g] Keith C. Gordon,[c,d] Stefano Stagni,[b,*] Massimiliano Massi[a,*]

[a] Department of Chemistry, Curtin University, Kent Street, Bentley WA 6102, Australia.

[b] Department of Industrial Chemistry, University of Bologna, viale del Risorgimento 4, 40126 Bologna, Italy.

[c] Department of Chemistry, University of Otago, Union Place, Dunedin, New Zealand.

[d] MacDiarmid Institute for Advanced Materials and Nanotechnology, New Zealand.

[e] Centre for Microscopy, Characterisation and Analysis, University of Western Australia, Crawley 6009 WA, Australia.

[f] Consorzio MIST E-R Via P. Gobetti 101, 40129 Bologna, Italy.

[g] Institute for Organic Synthesis and Photoreactivity, CNR, via Gobetti 101, 40129 Bologna.

Corresponding author email: Stefano.stagni@unibo.it; m.massi@curtin.edu.au

Abstract

The irreversible reaction of methyl triflate with the neutral Re(I) tetrazolato complexes of the type *fac*-[Re(**diim**)$(CO)_3$(**L**)], where **diim** is either 1,10-phenanthroline or 2,2'-bipyridine and **L** is a *para* substituted 5-aryltetrazolate, yielded the corresponding cationic methylated complexes. While methylation occurred regioselectively at the N4 position of the tetrazole ring, the cationic

complexes were found to exist in solution as an equilibrating mixture of linkage isomers, where the Re(I) centre was bound to either the N1 or N2 atom of the tetrazole ring. The existence of these isomers was highlighted both by NMR and X-ray crystallography studies. On the other hand, the two isomers appeared indistinguishable by means of IR, UV-Vis and luminescence spectroscopy. The prepared cationic complexes are all brightly phosphorescent in fluid and rigid solutions, with emission originating from triplet metal-to-ligand charge transfer excited states. Compared to their neutral precursors, which are emitting from admixtures of triplet metal-to-ligand and ligand-to-ligand charge transfer states, the methylated complexes exhibit blue-shifted emission characterised by elongated excited state lifetimes and increased quantum yields. The nature of the excited states for both the neutral and methylated complexes was probed by means of resonance Raman spectroscopy and with the aid of Time-Dependent Density Functional Theory calculations. Lastly, both the neutral and methylated species were used as emitting phosphors in the fabrication or Organic Light Emitting Devices and Light Emitting Electrochemical Cells.

Introduction

The excited states of tricarbonyl Re(I) complexes are the origin of rich and well documented photophysical and photochemical properties. [1,2] These advantageous properties have driven the investigation of these complexes in a multitude of applied fields encompassing optical devices,[3] biological markers[4-6] as well as photocatalysis. [7,8] In general, this class of complexes is centred around the *fac*-[Re(**diim**)$(CO)_3$(**L**)]$^{0/+}$ formulation, where **diim** represents a variety of functionalised diimine-type chelating ligand, such as 1,10-phenanthroline (**phen**) or 2,2'-bipyridine (**bipy**), and **L** is a monodentate ancillary ligand. The lowest excited state manifold of these complexes originates in general from metal-to-ligand charge transfer (MLCT) transitions with a variable degree of admixture from ligand-to-ligand charge transfer (LLCT) transitions, depending on the chemical nature of the ancillary ligand **L**.[1] The emission from these charge transfer states has

been ascribed to long-lived phosphorescence, which is promoted by the spin-orbit coupling of the Re(I) centre favouring intersystem crossing from the singlet ^{1}MLCT excited state to the more stable triplet ^{3}MLCT excited state. [9-11] The relative energy of the spin-forbidden radiative decay ^{3}MLCT$\rightarrow$GS can be opportunely tuned by chemical modifications of the diimine and ancillary ligands.[1] The excited state lifetime (τ) and photoluminescent quantum yield (Φ) of the complexes are in general linked to the energy of the emitted photons, displaying trends that are consistent with the energy gap law.[12] In fact, cationic complexes such as *fac*-[Re(**diim**)$(CO)_3$(**L**)]$^+$, where **L** is a neutral ligand such as pyridine, exhibit blue-shifted emission, elongated τ, and higher Φ.[1]

We have previously investigated the photophysical properties of neutral *fac*-[Re(**diim**)$(CO)_3$(**L**)] complexes, where **L** represents an anionic 5-aryltetrazolato ligand and **diim** was alternated between **phen** and **bipy**.[13] The emission of these compounds was found to originate from admixtures of ^{3}MLCT and ^{3}LLCT, with a strong contribution from the HOMO-type orbitals from the negatively charged tetrazole heterocycle. Furthermore, we have shown in our studies how the photophysical properties of these complexes can be significantly changed, in a reversible manner, when the tetrazole ring becomes protonated via addition of triflic acid.[14] The protonated complexes in fact display emission profiles blue-shifted by about 50 nm along with an elongation of the τ from few hundreds of ns to few μs and a four- to six-fold increase in Φ. In fact, we have shown how this reversible modulation of the photophysical properties of these Re(I) tetrazolato complexes, achieved by varying the electron density on the tetrazole ring thus affecting the stabilisation of the HOMO-type orbitals, is a general feature of phosphorescent Ru(II), Ir(III) and Pt(II) phosphorescent complexes. [14,15]

Prompted by the reversible proton-induced modulation of the photophysical properties of the Re(I) tetrazolato complexes (including significant improvement of their Φ), we endeavoured to isolate cationic Re(I) tetrazolato complexes obtained by irreversible reaction of the tetrazole ring with an electrophilic reagent, e.g. CH_3^+ (Scheme 1). While the reactivity of the complexes versus triflic acid

or methyl triflate and the variation of the photophysical properties on passing from the neutral to the cationic species followed analogous trends, the irreversible methylation of the complexes was found to result in an equilibrating mixture of two linkage isomers, where the Re(I) centres were coordinated to the N1 or N2 atom of the tetrazole ring and the methyl group was bound in all cases to the N4 atom. Resonance Raman spectroscopy was used to probe and compare the nature of the excited states in the neutral and methylated complexes, with the results corroborated by computational calculations. The high solution luminescence quantum yields and relatively short triplet lifetimes render this new family of rhenium(I) complexes of interest for testing as triplet-harvesting phosphors. [16-19] Therefore, the neutral and methylated tetrazolato complexes were explored for the first time as emissive dyes in the fabrication of Organic Light Emitting Devices (OLEDs) and Light Emitting Electrochemical Cells (LEECs), respectively.

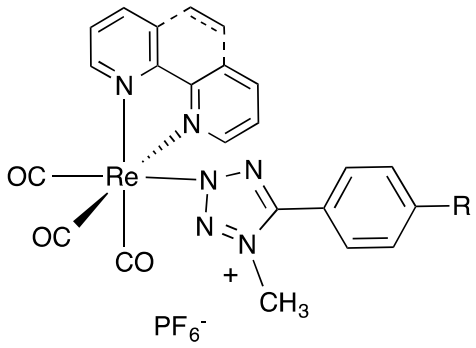

R = H, CHO, $COOCH_3$ L = **Tph**CH_3, **Tbdz**CH_3, **Tmeb**CH_3

Scheme 1. Formulation of the methylated *fac*-[Re(**diim**)$(CO)_3$(**L**)][PF_6] complexes prepared in this work, where the **diim** ligand represents either 1,10-phenanthroline or 2,2'-bipyridine. Only the N2 linkage isomer is shown in the Scheme.

Results and Discussion

Synthesis and characterisation of the menthylated Re(I) complexes via IR and NMR spectroscopy

The preparation of the methylated Re(I) compounds described herein has been accomplished by the reaction of the neutral Re(I) precursors with a slight excess of methyl triflate in dichloromethane at -50 °C, followed by metathesis with NH_4PF_6, as illustrated in Scheme 2.

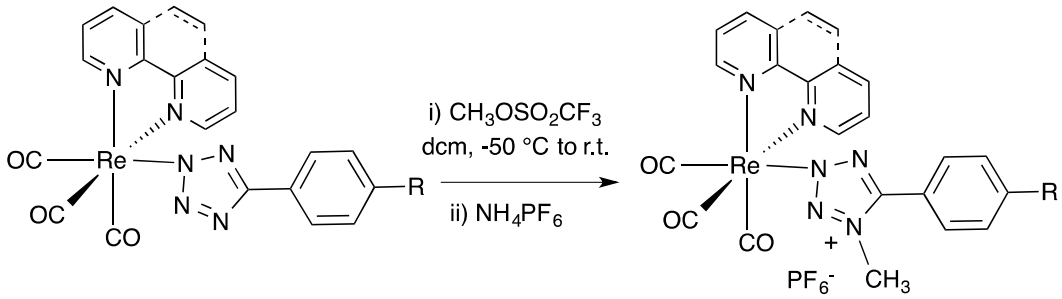

Scheme 2. Reaction and conditions for the preparation of the methylated *fac*-[Re(**diim**)$(CO)_3$(**L**)][$PF]_6$ complexes.

All the methylated complexes could be isolated in acceptable purity by simple reprecipitation from the corresponding crude mixtures and no column chromatography work-up was required. The resulting complexes were at first characterised by performing Electro-Spray Ionisation Mass Spectrometry (ESI-MS) and solid state IR spectroscopy experiments. Increases in the carbonyl stretching band frequencies in the 2040 to 1880 cm^{-1} region, [20-22] confirmed the successful methylation of the complexes. These changes, analogous to those observed in the case of the protonation,[14] are again rationalised by a decrease in electron density on the tetrazole ring thus disfavouring Re-CO π-backbonding.

The ^1H NMR spectra of the methylated Re(I) complexes indicated their occurrence as almost equimolar mixtures of two isomeric species. The two isomers were evidenced by the clear splitting

of the **phen** and **bipy** signals into two sets of four peaks. The molar ratios of the two complexes ranged between 1:0.65 to 1:1 depending on the specific methylated complex examined. Attempt to separate these isomers by column chromatography proved unsuccessful and the relative ratio stayed constant after each purification attempt. This behaviour pointed out to the rapid establishment in solution of equilibrium between the two isomers. The presence of two isomers was also confirmed by the ^{13}C NMR spectra. Specifically, for each complex it was possible to identify two distinct environments for the tetrazolic C arom (C_t) and four environments corresponding to the carbonyl ligands (Figure 1). The chemical shifts of each pair of C_t signals were always found at values below 160 ppm. These chemical shift values are indicative of poor interannular conjugation due to lack of coplanarity between the tetrazole and phenyl rings, [23,24] confirming substitution in position N4 of the tetrazole ring. As the spectra of all the complexes are analogous, it was concluded that the two isomeric species were linkage isomers where methylation occurred at the N4 atom of the tetrazole ring and coordination of the Re centre equilibrates between the N1 and N2 atoms (Scheme 3). The occurrence of this type of linkage isomers, which seems to be unique in the case of Re(I) tetrazolato complexes, was previously observed for dinuclear complexes where two Re(I) centres were simultaneously coordinated to the tetrazole ring.[25]

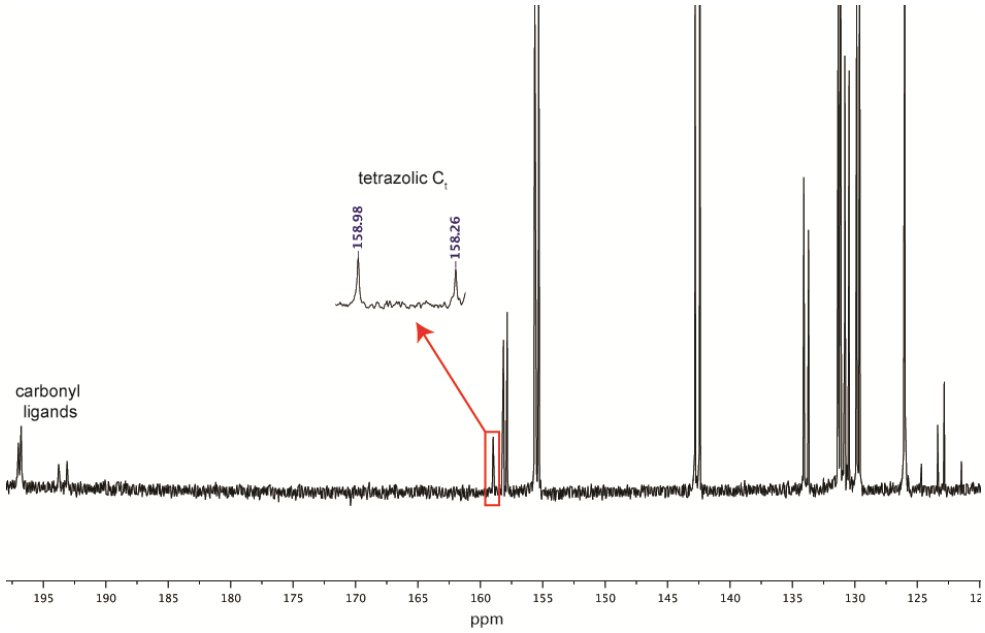

Figure 1. ^{13}C NMR spectrum of *fac*-[Re(**bipy**)$(CO)_3$(**Tph**CH_3)][PF_6] highlighting the two peaks corresponding to the tetrazolic C atom (C_t) of the N1 and N2 linkage isomers as well as the four peaks corresponding to the CO ligands in the 190-200 ppm region.

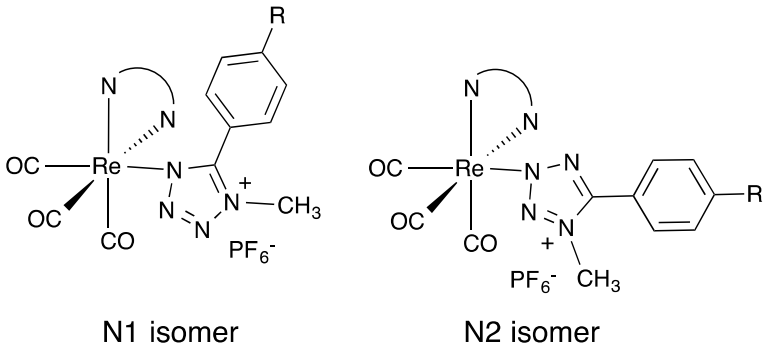

Scheme 3. Representation of the N1 and N2 linkage isomers for the methylated Re(I) complexes.

X-ray structural determination of the Re(I) methylated complexes as N1 and N2 linkage isomers

Further insights on the nature of the isomer species could be gained from the analysis of the molecular structures of all of the cationic complexes, which have been determined by single crystal X-ray diffractometry as their *fac*-[Re(**phen**)$(CO)_3$(**Tph**CH_3)][PF_6], *fac*-[Re(**bipy**)$(CO)_3$(**Tph**CH_3)][CF_3SO_3]•CH_2Cl_2, *fac*-[Re(**phen**)$(CO)_3$(**Tbdz**CH_3)][PF_6]•$CDCl_3$, *fac*-[Re(**bipy**)$(CO)_3$(**Tbdz**CH_3)][PF_6]•$CHCl_3$, *fac*-[Re(**phen**)$(CO)_3$(**Tmeb**CH_3)][PF_6] and *fac*-[Re(**bipy**)$(CO)_3$(**Tmeb**CH_3)][PF_6] salts (Figure 2 and ESI Figures S1-4). Selected bond lengths and angles are reported in Table 1. The Re centres in all the complexes display an octahedral geometry being coordinated to three CO ligands (in a *facial* arrangement), a *cis*-chelating diimine ligand (**bipy** or **phen**) and an aryl substituted methylated tetrazolate ring. Also, consistent with the analysis of the ^1H and ^{13}C NMR data, in all the complexes methylation occurred at the N4 position. Apart from these expected features, the analysis of the molecular structures established how the formation of the two distinct isomers is related to the different positions of the tetrazole ring to which the Re(I) fragment is coordinated. Indeed, whereas the tetrazolate ligand is bound to Re(I) through the

expected N2 position in the complexes *fac*-[Re(**bipy**)$(CO)_3$(**Tph**CH_3)]$^+$ and *fac*-[Re(**bipy**)$(CO)_3$(**Tbdz**CH_3)]$^+$, the coordination of the Re(I) fragment occurs via the N1 position for the complexes *fac*-[Re(**phen**)$(CO)_3$(**Tph**CH_3)]$^+$, *fac*-[Re(**phen**)$(CO)_3$(**Tbdz**CH_3)]$^+$, *fac*-[Re(**phen**)$(CO)_3$(**Tmeb**CH_3)]$^+$ and *fac*-[Re(**bipy**)$(CO)_3$(**Tmeb**CH_3)]$^+$. This latter feature represents a major difference compared to the analogous protonated Re(I) tetrazolato complexes where the coordination of the Re(I) centre occurred exclusively at the tetrazole N2 position.

The existence of the two linkage isomers in equilibrium was further confirmed upon isolating batches of single crystals, as the N1 or N2 isomer depending on the specific complex, and verifying that the ^{1}H NMR spectra appeared again as mixtures of the two species in identical stoichiometric ratios as previously reported.

The bonding parameters are very similar for all of the Re(I) methylated complexes (Table 1) and comparable to those reported for the analogous protonated species.[14] In all cases, the tetrazolate and aryl rings are not coplanar with the torsion angle between their planes ranging from -85.8(4) to 140.2(9)°, corresponding to absolute values (reduced in the 0-90° range) from 39.8 to 87.0°. For comparison, an absolute value (reduced in the 0-90° range) of 0° indicates perfect coplanarity between the tetrazolate and aryl ring. The fact that the experimental values are rather spread suggests that the relative orientation of the tetrazolate and aryl rings in the solid state are mainly determined by packing effects. It is noteworthy that the deviation from planarity is greater for the N1 isomers (reduced absolute torsion angles 72.0-87.0°) than in the case of the N2 ones (reduced absolute torsion angles 39.8 and 47.9°). The orientation of the aryl substituted methylated tetrazolate ligand relative to the Re(I) framework is rather different along the series of the complexes, as indicated for instance by the C(2)-Re(1)-N(1,2)-N(2,1) torsion angle (Table 3), which ranges from 29.9(9) to 71(6)°. Also in this case it is likely that packing forces determine the conformation found in the solid state, whereas free rotation around the Re(1)-N(1,2) bond occurs in solution, as evidenced by the higher symmetry of the **phen** or **bipy** ligand found by ^{1}H and ^{13}C NMR in solution.

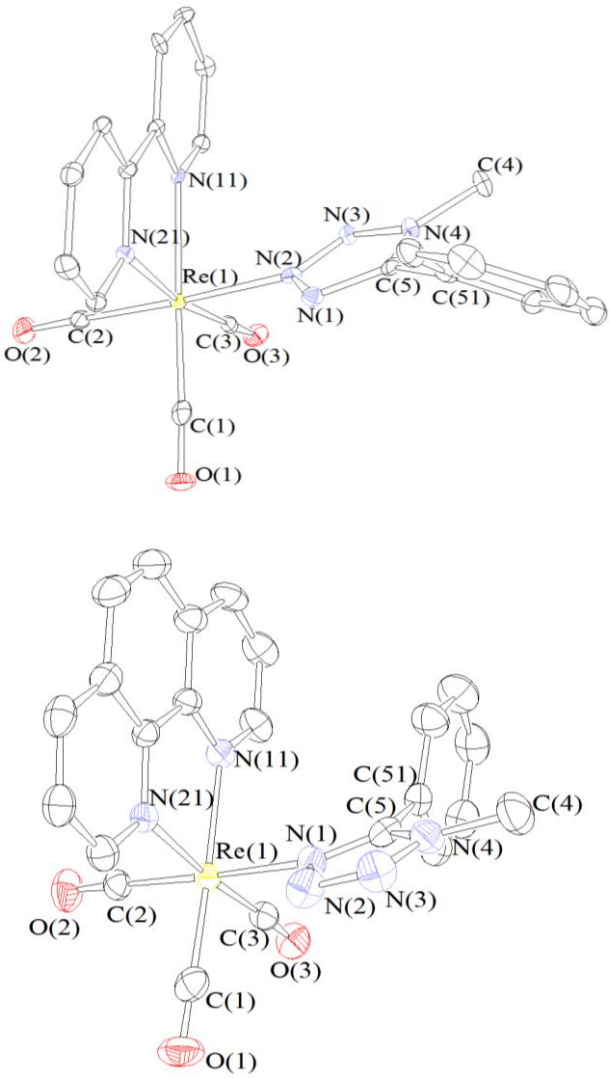

Figure 2. X-ray crystal structures of the N2 linkage isomer of *fac*-[Re(**bipy**)$(CO)_3$(**Tph**CH_3)]$^+$ (top) and the N1 linkage isomer of *fac*-[Re(**phen**)$(CO)_3$(**Tph**CH_3)]$^+$ (bottom) with key atoms labelled. Displacement ellipsoids are at 30% probability level. H-atoms and PF_6^- anions are omitted for clarity.

Table 1. Selected bond lengths (Å) and angles (°) for *fac*-[Re(**phen**)$(CO)_3$(**Tph**CH_3)]$^+$ (**1**), *fac*-[Re(**bipy**)$(CO)_3$(**Tph**CH_3)]$^+$ (**2**), *fac*-[Re(**phen**)$(CO)_3$(**Tbdz**CH_3)]$^+$ (**3**), *fac*-[Re(**bipy**)$(CO)_3$(**Tbdz**CH_3)]$^+$ (**4**), *fac*-[Re(**phen**)$(CO)_3$(**Tmeb**CH_3)]$^+$ (**5**) and *fac*-[Re(**bipy**)$(CO)_3$(**Tmeb**CH_3)]$^+$ (**6**).

	(**1**)	(**2**)	(**3**)	(**4**)	(**5**)	(**6**)
Re(1)-C(1)	1.916(7)	1.916(10)	1.921(9)	1.939(8)	1.930(3)	1.9277(10)
Re(1)-C(2)	1.913(6)	1.927(9)	1.923(9)	1.918(9)	1.936(3)	1.9268(10)
Re(1)-C(3)	1.915(5)	1.914(9)	1.939(9)	1.908(8)	1.926(3)	1.9198(10)
Re(1)-N(1,2)[a]	2.200(5)	2.170(7)	2.189(6)	2.167(6)	2.204(2)	2.1974(8)
Re(1)-N(11)	2.170(4)	2.158(6)	2.162(6)	2.172(6)	2.189(3)	2.1666(8)
Re(1)-N(21)	2.171(4)	2.166(7)	2.166(6)	2.172(6)	2.178(3)	2.1766(8)
C(1)-O(1)	1.151(7)	1.165(11)	1.152(9)	1.140(9)	1.145(4)	1.1495(12)
C(2)-O(2)	1.146(7)	1.136(11)	1.150(9)	1.142(11)	1.150(4)	1.1430(13)
C(3)-O(3)	1.163(5)	1.153(11)	1.140(9)	1.157(9)	1.161(4)	1.1519(12)
N(1)-N(2)	1.379(6)	1.344(10)	1.337(9)	1.347(7)	1.370(3)	1.3723(11)
N(2)-N(3)	1.293(7)	1.312(10)	1.293(9)	1.305(8)	1.284(3)	1.2875(12)
N(3)-N(4)	1.337(6)	1.346(10)	1.373(10)	1.335(8)	1.347(3)	1.3458(12)
N(1)-C(5)	1.310(7)	1.327(11)	1.331(10)	1.320(9)	1.329(3)	1.3239(12)
N(4)-C(5)	1.338(6)	1.341(11)	1.310(10)	1.347(8)	1.343(3)	1.3343(12)
N(4)-C(4)	1.467(7)	1.464(11)	1.465(11)	1.470(9)	1.458(4)	1.4611(13)
C(5)-C(51)	1.481(7)	1.460(12)	1.488(12)	1.456(10)	1.471(4)	1.4775(13)
Re(1)-C(1)-O(1)	178.5(6)	176.7(8)	176.5(8)	177.3(8)	178.9(3)	179.30(9)
Re(1)-C(2)-O(2)	178.1(6)	179.1(9)	177.6(7)	178.8(8)	178.1(3)	177.99(9)
Re(1)-C(3)-O(3)	176.4(4)	177.6(8)	176.4(8)	178.9(7)	179.3(3)	177.54(9)
C(1)-Re(1)-N(11)	172.0(2)	172.0(3)	173.6(3)	171.9(3)	175.41(12)	173.42(4)
C(2)-Re(1)-N(1,2)[a]	175.1(2)	176.9(3)	178.5(3)	177.8(3)	175.16(10)	177.18(4)
C(3)-Re(1)-N(21)	174.78(17)	171.0(3)	172.7(3)	174.1(3)	171.54(12)	171.44(4)
N(11)-Re(1)-N(21)	76.00(16)	75.5(3)	76.0(2)	75.1(2)	75.74(12)	75.19(3)

Sum angles at N_4C	540.0(11)	540.1(16)	540.0(16)	540.0(12)	540.1(4)	540.01(18)
Sum angles at C(5)	360.1(9)	360.0(13)	360.0(13)	360.1(11)	360.0(3)	360.00(14)
Angle between the N_4C and C_6 rings	108.0(7)	132.1(9)	87.0(2)	140.2(9)	-85.8(4)	-82.8(2)
Angle between the N_4C and C_6 rings normalised in the 0-90° range	72.0(7)	47.9(9)	87.0(2)	39.8(9)	85.8(4)	82.8(2)
C(2)-Re(1)-N(1,2)-N(2,1)[a, b]	44(3)	71(6)	44.4(2)	29.9(9)	40.0(14)	35.9(8)

[a] N(1,2) refers to N(1) for **1**, **3**, **5** and **6**; N(1,2) refers to N(2) for **2** and **4**.

[b] N(2,1) refers to N(2) for **1**, **3**, **5** and **6**; N(2,1) refers to N(1) for **2** and **4**.

Photophysical Properties

The relevant absorption and emission data of all complexes, as N1 and N2 linkage isomer mixtures, from dilute dichloromethane solutions (ca. 10^{-5} M) are listed in Table 2. The absorption profiles of the Re(I) species are analogous and display intense ligand centered (LC) π-π* transitions occurring in the 250-350 nm region followed by weaker charge transfer (CT) bands above 350 nm. When compared to the initial neutral complexes,[13] the UV-vis absorption spectra of the cationic isomeric pairs display a more or less evident (due to the broad nature of the bands) hypsochromic shift of the MLCT transition, which is accompanied by an analogous variation of the LC-based absorption bands (see Figure 3, where the absorption spectrum of *fac*-[Re(**phen**)$(CO)_3$(**Tbdz**CH_3)]$^+$ is reported as exemplar and in comparison with its neutral precursor; see ESI Figures S5-6 for the remaining complexes). Again, the trend is consistent with the reduction of electron density on the tetrazole ring with consequent stabilisation of the HOMO-type orbitals.

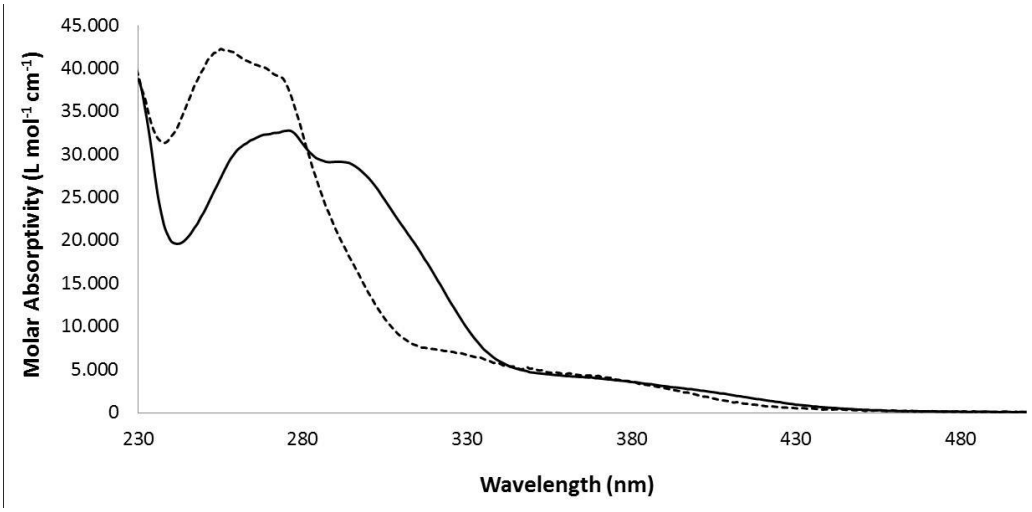

Figure 3: Absorption profiles of the neutral *fac*-[Re(**phen**)$(CO)_3$(**Tbdz**)] (solid line) and cationic *fac*-[Re(**phen**)$(CO)_3$(**Tbdz**CH_3)]$^+$ (dashed line) obtained from ca. 10^{-5} M dichloromethane solutions.

Table 2. Summary of the photophysical data for all the methylated Re(I) complexes, as mixtures of N1 and N2 linkage isomers.

	Absorption	**Emission (298 K)**						**Emission (77 K)**	
	λ [nm] ($10^4\varepsilon$) [M^{-1} cm^{-1}]	λ [nm]	τ^a [μs]	τ_b [μs]	Φ_a	Φ_b	k_r^a (10^6 s^{-1})	k_{nr}^a (10^6 s^{-1})	λ [nm]	τ [μs]
fac-[Re(**phen**)$(CO)_3$(**Tph**CH_3)]$^+$	256 (3.93) 276 (3.83) 365 (0.68)	536	2.0 2	1.0 0 0 0 0 0					499	2.8 0
fac-[Re(**bipy**)$(CO)_3$(**Tph**CH_3)]$^+$	252 (5.22) 319 (2.56) 350 (1.20)	546	1.0 0	0.0 0 0 0 0 0					449	0.0

	Absorption λ [nm] ($10^4\varepsilon$) [M^{-1} cm^{-1}]	Emission (298 K) λ [nm]	τ^a [µs]	τ^b [µs]	Φ^a	Φ^b	k_r (10^6 s^{-1})	k_{nr} (10^6 s^{-1})	Emission (77 K) λ [nm]	τ [µs]
				1	6	2	60	40		5[c]
fac-[Re(**phen**)$(CO)_3$(**Tbdz**CH_3)]$^+$	256 (4.22) 331 (0.67) 366 (0.43)	536	3.37	1.30	0.53	0.25	0.157	0.139	492	10.90
fac-[Re(**bipy**)$(CO)_3$(**Tbdz**CH_3)]$^+$	246 (3.98) 314 (1.5) 350 (0.5)	546	0.99	0.63	0.48	0.28	0.485	0.525	508	4.15
fac-[Re(**phen**)$(CO)_3$(**Tmeb**CH_3)]$^+$	254 (4.64) 333 (0.78) 380 (0.41)	538	3.20	1.40	0.57	0.23	0.178	0.134	508	9.13
fac-[Re(**bipy**)$(CO)_3$(**Tmeb**CH_3)]$^+$	265 (4.14) 320 (1.28) 350 (0.47)	546	1.02	0.64	0.34	0.20	0.333	0.647	500	4.38

fac-[Re(**phen**)(CO)$_3$(**Tph**CH$_3$)]$^+$	256 (3.93) 276 (3.83) 365 (0.68)	53 6	2.02	1.2 0	0.50	0.28	0.25 0	0.250	492	9.8 0
fac-[Re(**bipy**)(CO)$_3$(**Tph**CH$_3$)]$^+$	252 (5.22) 319 (2.56) 350 (1.20)	54 6	1.00	0.6 1	0.36	0.22	0.36 0	0.640	490	4.0 5[c]
fac-[Re(**phen**)(CO)$_3$(**Tbdz**CH$_3$)]$^+$	256 (4.22) 331 (0.67) 366 (0.43)	53 6	3.37	1.3 0	0.53	0.25	0.15 7	0.139	492	10. 90
fac-[Re(**bipy**)(CO)$_3$(**Tbdz**CH$_3$)]$^+$	246 (3.98) 314 (1.5) 350 (0.5)	54 6	0.99	0.6 3	0.48	0.28	0.48 5	0.525	508	4.1 5
fac-[Re(**phen**)(CO)$_3$(**Tmeb**CH$_3$)]$^+$	254 (4.64) 333 (0.78) 380 (0.41)	53 8	3.20	1.4 0	0.57	0.23	0.17 8	0.134	508	9.1 3

fac-[Re(**bipy**)(CO)$_3$(**Tmeb**CH$_3$)]$^+$	265	54	1.02	0.6	0.34	0.20	0.33	0.647	500	4.3
	(4.14)	6		4			3			8
	320									
	(1.28)									
	350									
	(0.47)									

[a] Measured from degassed solution; [b] measured from air-equilibrated solution; [c] the decay was best fitted with a biexponential function with a minor component (16%) at 8.42 μs.

In dilute dichloromethane solution at room temperature, all the cationic methylated complexes are brightly emissive and display broad and structureless bands that appear blue-shifted when compared to those of the parent neutral complexes (see Figure 4, where the emission spectrum of *fac*-[Re(**phen**)(CO)$_3$(**Tph**CH$_3$)]$^+$ is reported as exemplar and in comparison with its neutral precursor; see ESI Figures S7-9 for the remaining complexes). The emission profiles are independent from the excitation wavelength used. The emission is here ascribed to phosphorescence from charge transfer states of triplet multiplicity, ^{3}CT, similarly to the previously reported neutral and protonated Re(I) tetrazolato complexes. [13,14] In fact, the excited state lifetime τ and quantum yield Φ are sensitive to the presence of dissolved O_2 (Table 2). At 77 K, the emission profile appears blue-shifted as a consequence of rigidochromism (Figures S7-9) and the values of τ and Φ increase due to lack of vibrational and collisional quenching.[26] Noteworthy, the photophysical properties of the N1 and N2 linkage isomers appear to be essentially identical, a fact that is supported by the presence of only one band in the emission profile and by the satisfactorily monoexponential fitting of the excited state decay. In the parent neutral complexes the photophysical characteristics were modified by the specific chemical nature of the aryltetrazolato ligand coordinated to the Re(I) centre (e.g. variations of the substituent in the *para* position of the phenyl ring),[13] however, upon methylation all the complexes display very similar photophysical characteristics, with variation only dictated by the identity of the diimine ligand. This trend supports the fact that, in the methylated complexes, the

^{3}LLCT contribution to the excited state has been lost due to the stabilisation of the tetrazole π electrons. The emissive excited state therefore becomes almost exclusively of ^{3}MLCT in nature (Re→**diim**) and independent of the contribution from the tetrazole ligand. The increase in the values of τ and Φ upon methylation is mostly rationalised by a decreased non-radiative decay k_{nr} caused by the increased relative energy of the ^{3}MLCT excited state, as predicted by the energy gap law.[12]

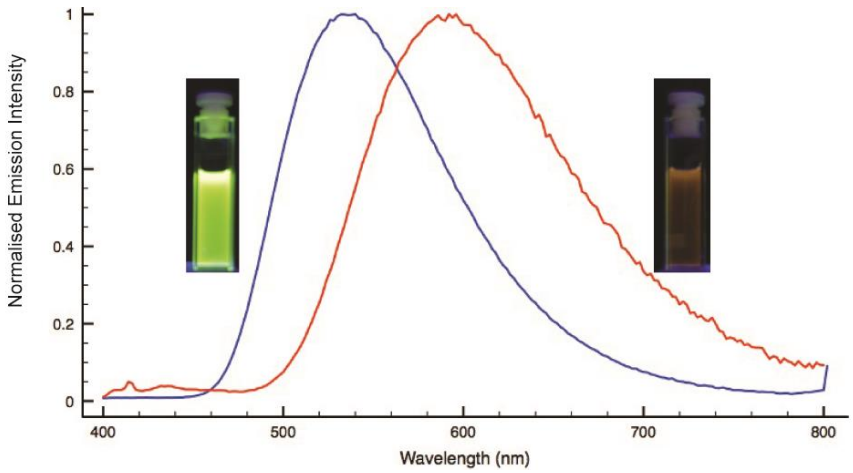

Figure 4. Normalised emission profiles of *fac*-[Re(**phen**)(CO)$_3$(**Tph**CH$_3$)]$^+$ (red trace) compared to that of the neutral precursor *fac*-[Re(**phen**)(CO)$_3$(**Tph**)] (black trace).

TD-DFT investigation

Time-Dependent Density Functional Theory (TD-DFT) and resonance Raman were used to further probe the changes in the photophysical properties upon methylation of the complexes. Since all complexes exhibited analogous behaviour, this investigation was carried out on those complexes with a bound **phen** ligand. Electron transition densities were calculated from the TD-DFT data to quantify the extent to which the methylated aryltetrazolato ligand contributes to the MLCT transitions for both the N1 and N2 isomers (see Table 3 for *fac*-[Re(**phen**)(CO)$_3$(**Tph**CH$_3$)]$^+$ used as exemplar; the other complexes are reported in the ESI Tables S1-2). The N1 and N2 isomers are predicted to give indistinguishable electronic spectra. The N1 isomer is calculated to be slightly

higher in energy than the N2 isomer by 4.0 to 8.5 kJ/mol depending on the substituent attached in the *para* position of the phenyl ring. As discussed previously, the lowest absorption band in the neutral complexes is composed of combined MLCT-LLCT transitions due to significant mixing of rhenium and tetrazole orbitals.[14] The lowest energy calculated transition is mostly HOMO to LUMO with nearly half of the electron density originating on the ancillary ligand while the LUMO is predominantly a π* orbital localised on the **phen** ligand. The HOMO-1 and HOMO-2 are based around the $Re(CO)_3$ fragment with an insignificant amount of overlap with the π system of the tetrazole ring, thus giving rise to pure MLCT bands as well. At higher energy, LC bands and MLCT bands with tetrazolate-based π* acceptor orbitals are found. The TD-DFT results for the methylated complexes are similar to those found for their previously discussed protonated counterparts, where the contribution from tetrazole orbitals to the MLCT transition is lost. The N1 and N2 isomers give very similar results. MLCT (Re→**phen**) transitions make up the lowest energy band of the methylated complexes. Unlike the neutral complexes there is an insignificant contribution from the tetrazolate π orbitals. At higher energy there are **phen**-based LC bands and MLCT (Re→**L**) transitions.

Table 3. Summary of TD-DFT data for *fac*-[Re(**phen**)$(CO)_3$(**Tbdz**CH_3)]$^+$ and its neutral counterpart.

L=	Transition #	Wavelength (nm)	*f*	Orbital contributions	$Re(CO)_3$				Phen				L		
Tbdz	1	421	0.0527	HOMO->LUMO (94%)	54	→	5		5	→	94		42	→	0
	2	404	0.0144	H-1->LUMO (96%)	90	→	5		6	→	94		4	→	0
	3	386	0.0126	HOMO->L+1 (97%)	53	→	1		5	→	99		43	→	0
	4	382	0.0001	H-2->LUMO (96%)	91	→	5		2	→	94		7	→	0
	5	365	0.0179	H-1->L+1 (94%)	89	→	1		7	→	99		4	→	0
	6	345	0.0002	H-2->L+1 (97%)	91	→	1		2	→	99		7	→	0
	7	343	0.0584	H-3->LUMO (90%)	37	→	5		10	→	94		54	→	0
	8	333	0.0001	H-4->L+2 (94%)	0	→	1		0	→	0		100	→	99
	9	330	0.4102	HOMO->L+2 (96%)	53	→	1		5	→	0		43	→	99
	10	320	0.0113	H-3->L+1 (92%)	34	→	1		12	→	99		54	→	0
$TbdzCH_3$ (N1)	1	390	0.0018	HOMO->LUMO (98%)	89	→	7		6	→	92		4	→	2
	2	371	0.0647	H-2->LUMO (18%), H-1->LUMO (75%)	82	→	6		17	→	91		2	→	3
	3	362	0.0328	H-2->LUMO (77%), H-1->LUMO (12%)	92	→	6		7	→	91		1	→	4
	4	347	0.0773	H-1->LUMO (10%), HOMO->L+1 (71%), HOMO->L+2 (13%)	87	→	2		8	→	73		4	→	24
	5	344	0.0000	H-4->L+1 (18%), H-4->L+2 (73%)	0	→	0		0	→	34		100	→	65
	6	337	0.0128	HOMO->L+1 (15%), HOMO->L+2 (83%)	89	→	0		6	→	29		4	→	71
	7	336	0.0214	H-1->L+1 (82%), H-1->L+2 (8%)	76	→	2		22	→	75		2	→	23
	8	327	0.0033	H-1->L+2 (85%), H-1->L+1 (8%)	79	→	0		19	→	27		2	→	73
	9	326	0.0059	H-2->L+1 (84%), H-2->L+2 (9%)	94	→	2		5	→	74		0	→	24
	10	316	0.0009	H-2->L+2 (86%), H-2->L+1 (8%)	95	→	0		5	→	26		0	→	74
$TbdzCH_3$ (N2)	1	388	0.0013	H-1->LUMO (98%)	92	→	6		7	→	93		1	→	0
	2	381	0.0816	H-2->LUMO (10%), HOMO->LUMO (85%)	81	→	6		14	→	93		5	→	0
	3	371	0.0230	H-2->LUMO (88%), HOMO->LUMO (9%)	96	→	6		4	→	93		1	→	0
	4	348	0.0001	H-4->L+1 (91%)	0	→	0		0	→	3		100	→	96
	5	346	0.0215	HOMO->L+2 (91%)	77	→	2		18	→	98		6	→	0
	6	346	0.0467	H-1->L+2 (89%)	89	→	2		10	→	98		1	→	0
	7	336	0.0116	HOMO->L+1 (97%)	79	→	0		15	→	1		6	→	99
	8	333	0.0075	H-1->L+1 (96%)	92	→	0		7	→	1		1	→	99
	9	333	0.0022	H-2->L+2 (96%)	97	→	1		3	→	98		0	→	0
	10	320	0.0002	H-2->L+1 (96%)	97	→	0		3	→	1		0	→	99

Raman and resonance Raman spectroscopy

Raman spectroscopy was used to confirm the switch from mixed MLCT/LLCT transitions for the neutral complexes to pure MLCT in the case of the methylated complexes. Non-resonant spectra were recorded at 1064 nm in the solid state and compared to spectra predicted by DFT in order to assign the vibrational modes. Simulated spectra of the N1 and N2 isomers are nearly indistinguishable (see Figure 5 for *fac*-[Re(**phen**)$(CO)_3$(**Tbdz**CH_3)]$^+$ used as exemplar; the other complexes are reported in Figures S10-11).

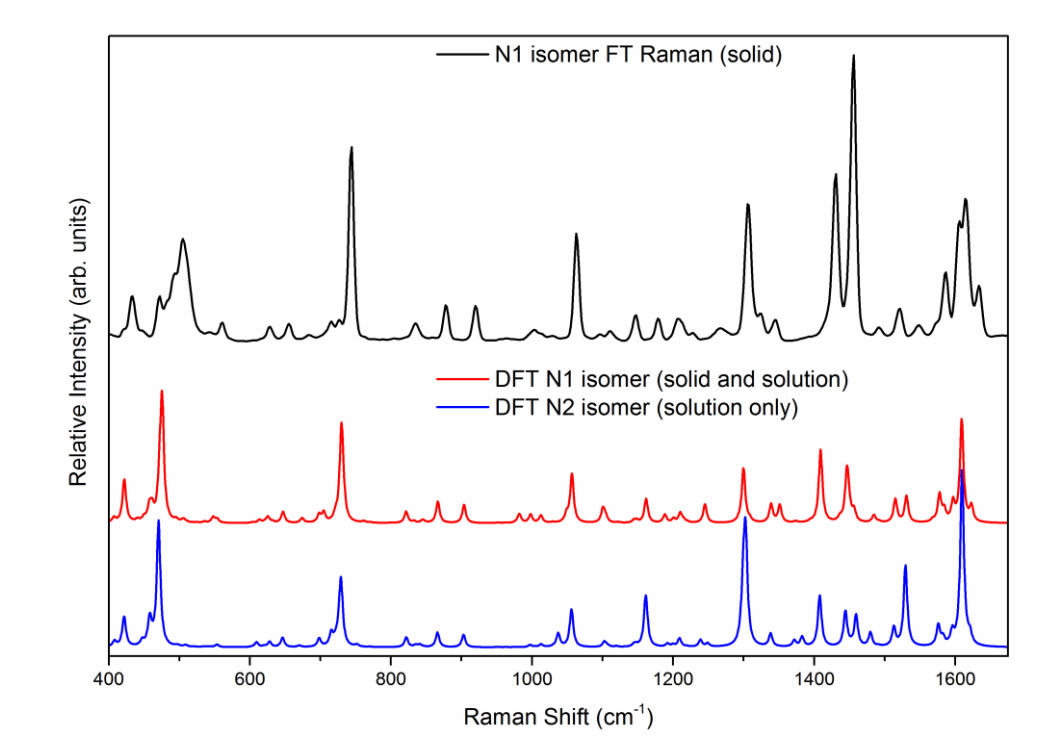

Figure 5. FT-Raman of solid *fac*-[Re(**phen**)$(CO)_3$(**Tbdz**CH_3)]$^+$ (black trace) and calculated Raman spectra of both N1 (red trace) and N2 (blue trace) coordinated isomers.

Resonance Raman spectra were acquired in dichloromethane solution where both methylated isomers are present (see Figures 6 and 7 for the neutral *fac*-[Re(**phen**)$(CO)_3$(**Tbdz**)] and cationic *fac*-[Re(**phen**)$(CO)_3$(**Tbdz**CH_3)]$^+$ used as exemplars; the other complexes are reported in ESI Figures S12-14). Resonant spectra at 351 nm excitation probed the region between the MLCT and LC transitions and vibrations of both the **phen** and tetrazolato **L** ligands are enhanced. As the

excitation wavelength is increased to 413 nm, the MLCT band is probed exclusively. The 413 nm spectra of the neutral complexes show enhancement of the same modes found at 351 nm excitation with stronger **phen** modes and somewhat weaker **L** modes. The tetrazolate modes are enhanced less strongly at longer wavelengths because the LC bands are no longer being probed. The methylated complexes show only enhancement of **phen** modes at 413 nm which is consistent with the assignment of this band as MLCT (Re→**phen**) in which the ancillary **L** ligand plays a minimal role as an electron donor or acceptor.

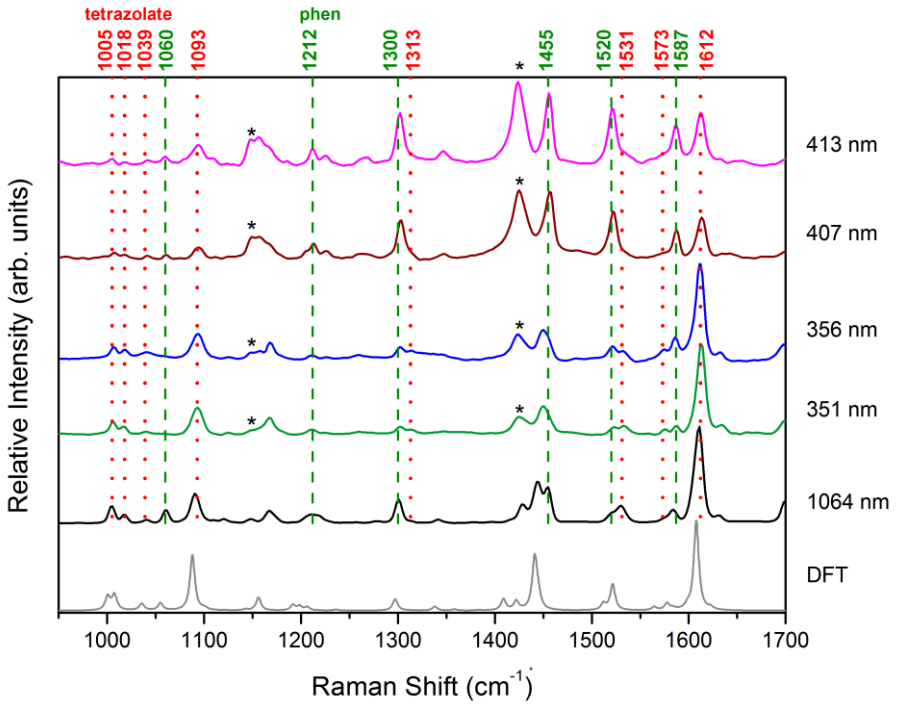

Figure 6. Raman spectra of the neutral *fac*-[Re(**phen**)$(CO)_3$(**Tbdz**)]. Tetrazolate modes are labelled with dotted lines and **phen** modes with dashed lines. Solvent bands are indicated by an asterisk (*).

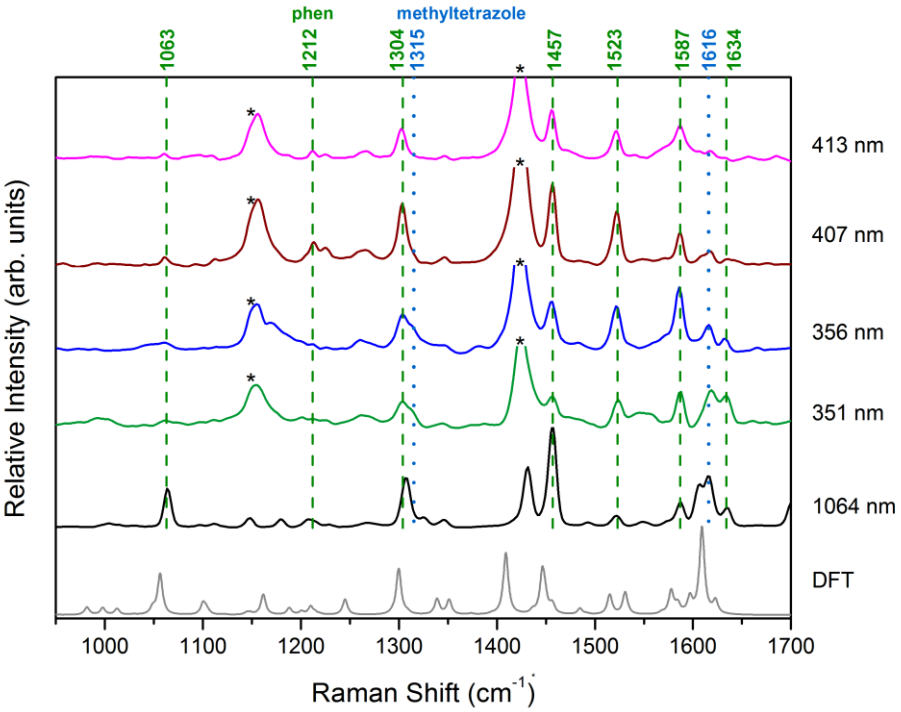

Figure 7. Raman spectra of the cationic *fac*-[Re(**phen**)$(CO)_3$(**Tbdz**CH_3)]$^+$. Methyltetrazole modes are labelled with dotted lines and **phen** modes with dashed lines. Solvent bands are indicated by an asterisk (*).

Fabrication and characterisation of OLED

In order to draw useful indications on how the neutral complexes will behave as the emitting layer in OLEDs, the luminescence properties of *fac*-[Re(**phen**)$(CO)_3$(**Tph**)] were evaluated in a polystyrene (PS) matrix at room temperature. Films with weight ratios 0.1% of Re(I) complex in PS and 100% Re(I) complex were investigated in order to determine self-quenching effects. The corresponding photophysical data for this study are reported in Table 4. The photoluminescence spectra of *fac*-[Re(**phen**)$(CO)_3$(**Tph**)] in neat film show a red-shifting effect of 16 nm. This difference could be expected due to the formation of aggregates in the solid state. [27-29]

Table 4. Photophysical data for the *fac*-[Re(**phen**)$(CO)_3$(**Tph**)] complex in polystyrene matrix (0.1% in PS) and in the neat film (100%).

τ [μs] 0.1% in PS	τ [μs] 100%	Φ 0.1% in PS	Φ 100%	λ [nm] 0.1% in PS	λ [nm] 100%
890 (24%) 2460 (76%)	330 (23%) 1000 (77%)	0.56	0.11	556	572

The complex *fac*-[Re(**phen**)$(CO)_3$(**Tph**)], blended with 1,3,5-tri(9H-carbazol-9-yl)benzene (TCP) at 10% by weight or 100% neat film, was investigated as the emitting layer in an OLED multilayer structure (Figure 8). The OLED based on a complex/TCP blended film as the emitting layer gave higher efficiency electroluminescence (EL). The EL spectra of these devices are shown in Figure 9 and the performance data summarised in Table 5. The EL profiles closely match the emission bands recorded from the PS matrix and as a neat film. No contribution to the EL emission from the TCP binder, the hole-transporting layer or electron-transporting layer is observed, indicating that the excitons are confined to the emissive layer and, localised on the phosphorescent *fac*-[Re(**phen**)$(CO)_3$(**Tph**)] complex prior to relaxation. The CIE (Commission Internationale

d'Eclairage) coordinates for these OLEDs fall between the green and red colors for the blend and neat film-based emitter, respectively (Table 7).

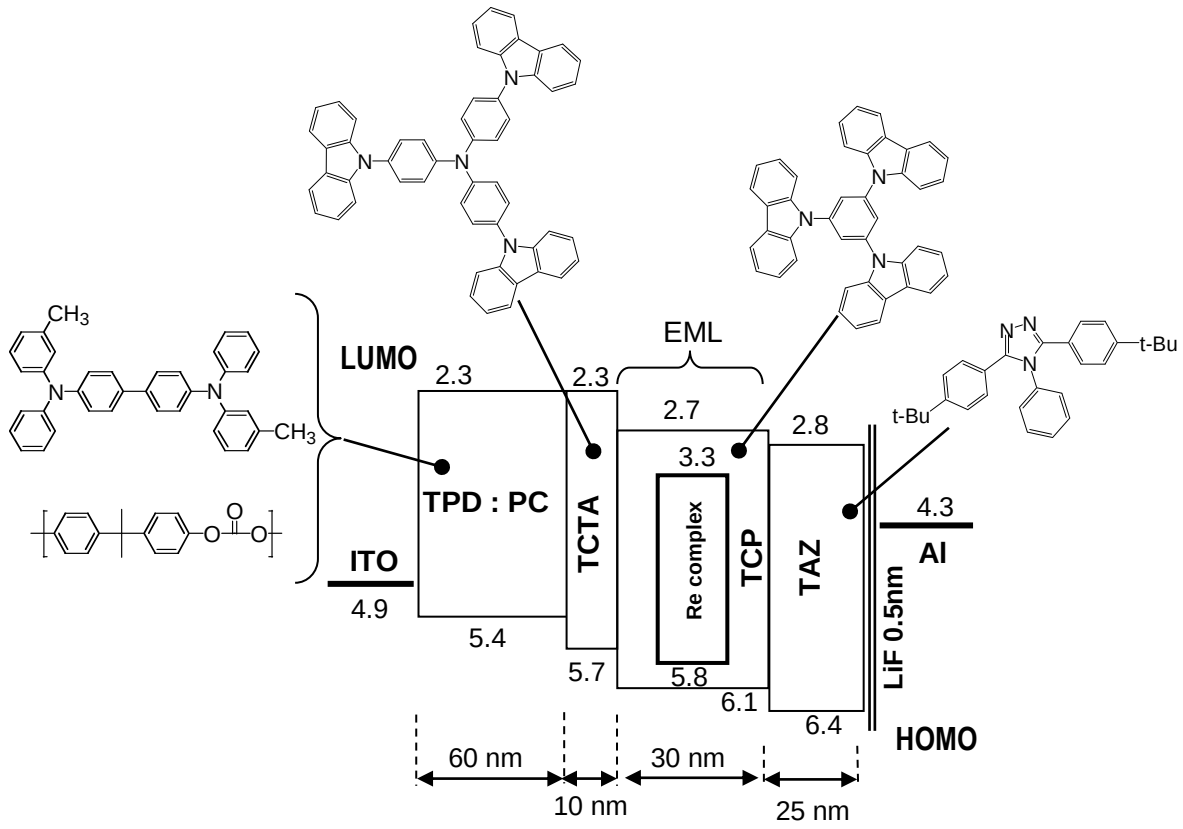

Figure 8. OLED architecture, molecular structures and electronic energy levels of the materials used. The energy values are derived from the redox potential measured by cyclic voltammetry (HOMO) and from the spectroscopic energy gap (LUMO).

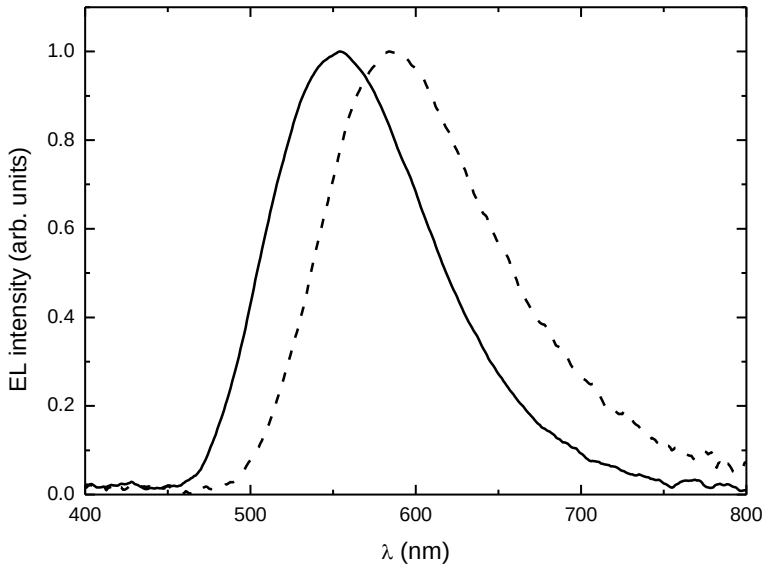

Figure 9. Electroluminescence spectra from the OLEDs fabricated with *fac*-[Re(**phen**)$(CO)_3$(**Tph**)] as the emissive phosphor at 10% Re in TCP (dashed line) and as 100% neat film (solid line).

Table 5. Performance of OLEDs having the *fac*-[Re(**phen**)$(CO)_3$(**Tph**)] in the emitting layer at concentrations of 10% and 100%.

EQE (j) [A cm^{-2}] 10%	EQE (j) [A cm^{-2}] 100%	λ [nm] 10%	λ [nm] 100%	CIE (x, y) 10%	CIE (x, y) 100%
7.1 ($5.6*10^{-6}$)	0.6 ($9.4*10^{-4}$)	555	584	0.41, 0.54	0.51, 0.47

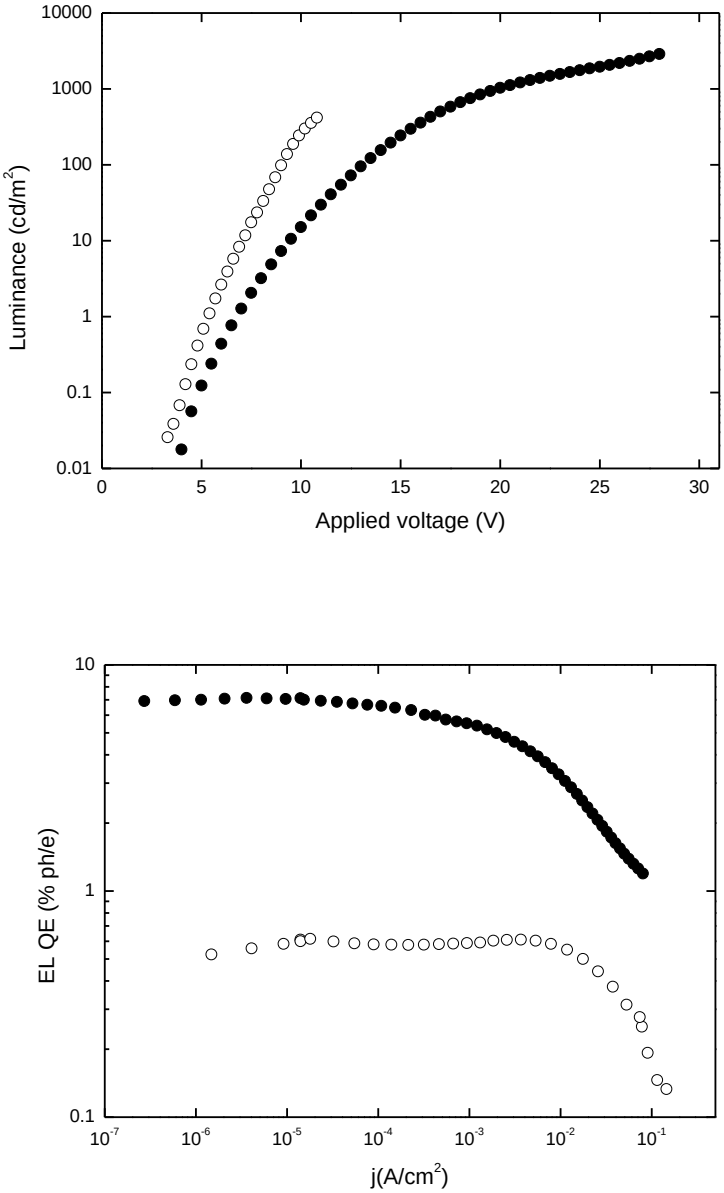

Figure 10. Luminance versus applied voltage (top) and External Quantum Efficiency (EQE) versus electric current density (bottom) for the OLEDs fabricated with *fac*-[Re(**phen**)$(CO)_3$(**Tph**)] as the emissive phosphor at 10% Re in TCP (full circles) and as 100% neat film (empty circles).

The luminance (L) as a function of driving voltage (V) and the external EL quantum efficiency (EQE) as a function of current density (j) are displayed in Figure 10. The maximum luminance reaches 4000 cd/m^2 at j ≈ 100 mA/cm^2 with maximum external quantum efficiency (EQE) = 7.1 %. These values are comparable to those reported for OLEDs with identical architecture fabricated

using *fac*-[Re(**phen**)$(CO)_3$Br] in the emissive layer.[30] A pronounced lowering in EQE was observed for OLED fabricated with 100% *fac*-[Re(**phen**)$(CO)_3$(**Tph**)] in the emissive layer.

Application in LEEC

The cationic complex *fac*-[Re(**phen**)$(CO)_3$(**Tph**CH_3)]$^+$ was used as phosphor in a LEEC-type device. The device was composed of an ITO anode covered with 40 nm thick PEDOT layer, 60 nm thick film of Re complex, and an aluminum cathode. The performance of the device was investigated by applying a voltage of 6, 7 and 8 V and corresponding parameters are presented in Table 6. The luminance versus operation time is presented in the ESI (Figure S15).

Table 6. Performance of LEEC having fabricated using *fac*-[Re(**phen**)$(CO)_3$(**Tph**CH_3)]$^+$ as the emissive phosphor.

U [V]	t_{on}[a] [min]	$t_{1/2}$[b] [min]	L_{max} [cd m^{-2}]	Current efficiency[c] [cd A^{-1}]	EL Φ (% ph/e)
6	167	840	0.6	0.02	0.006
7	46	190	3.4	0.04	0.013
8	9	40	14.0	0.06	0.020

[a] Time to reach maximum of the luminance (L_{max}); [b] time to reach half of the maximum luminance; [c] maximum value.

The studied LEEC emits yellow light and the electroluminescence spectrum (ESI Figure S16) displays a broad band stretching from 450 to 700 nm with the peak maximum at 535 nm and CIE coordinates x = 0.37 and y = 0.54. In this regard to increase the LEEC performance, a more systematic study of the charge carriers mobility and balancing is in progress using ionic liquid at different concentration in the active layer.[31]

Conclusions

Continuing our studies on the photophysical properties of Re(I) tetrazolato complexes, this work investigated their analogous cationic methylated species, obtained by irreversible methylation of the parent neutral *fac*-[Re(**diim**)$(CO)_3$(**L**)]. Unlike other examples of methylation reactions using Ru(II), Ir(III) or Pt(II) complexes, the obtained Re(I) species exist as an equilibrating mixtures of two linkage isomers, where the Re(I) centres are coordinated to either the N1 or N2 atoms of the tetrazole ring. This behaviour seems to suggest a reduction in the bond strength that is experience by the complex when the tetrazolato ligand becomes methylated and neutral in charge. These two linkage isomers can be clearly distinguished by means of ^{1}H and ^{13}C NMR. On the other hand, they have virtually identical properties when investigated by UV-vis, IR and emission spectroscopies. Methylation of the starting complexes clearly improves their photophysical properties in terms of increase of photoluminescence quantum yield, which is accompanied by an elongation of the excited state lifetime and blue-shift of the emission maxima. The identity of the excited state was probed by means of resonance Raman spectroscopy, highlighting how methylation of the tetrazole ligand removes the contribution of the tetrazole π orbitals from the composition of the HOMO. In fact, while the excited state in the neutral *fac*-[Re(**diim**)$(CO)_3$(**L**)] complexes is ascribed to an admixture of ^{3}MLCT and ^{3}LLCT, in the methylated complexes it becomes a pure ^{3}MLCT. Exploring the application of the Re(I) tetrazolato complexes in optical deviced, it was shown that the neutral complex *fac*-[Re(**phen**)$(CO)_3$(**Tph**)] can be successfully used as triplet-state emitter in the fabrication of efficient OLEDs. Furthermore, preliminary studies of first LEEC devices based on the cationic methylated *fac*-[Re(**phen**)$(CO)_3$(**Tph**CH_3)]$^{+}$ showed that these species may be successfully applied as emitting materials in this kind of electroluminescent devices.

Experimental Section

General considerations

All the reagents and solvents were obtained commercially (Aldrich) and used as received without any further purification. All the reactions were carried out under an argon atmosphere following Schlenk protocols. ESI-mass spectra were recorded using a Waters ZQ-4000 instrument (ESI-MS, acetonitrile as the solvent). IR spectra were recorded on a Perkin-Elmer Spectrum 2000 FT-IR spectrometer. Nuclear magnetic resonance spectra (consisting of ^{1}H, and ^{13}C experiments) were recorded using a Varian Mercury Plus 400 instrument (^{1}H, 400.1; ^{13}C, 101.0 MHz) at room temperature. ^{1}H and ^{13}C chemical shifts were referenced to residual solvent resonances; in some instances, the resonance signals for the CO ligands in the ^{13}C spectra were too weak to be precisely located. Melting points were determined using a BI Barnsted Electrothermal 9100 apparatus. Elemental analyses were performed by Mr. Robert Herman at the Department of Chemistry, Curtin Univrsity, or by Dr Thomas Rodemann at the Central Science Laboratory, University of Tasmania.

Synthetic details

The synthesis of the neutral complexes *fac*-[Re(**diim**)$(CO)_3$(**L**)] was reported elsewhere.[13] Methylation of the *fac*-[Re(**diim**)$(CO)_3$(**L**)] complexes was carried out following procedures adapted from previously published works.[24] The complex *fac*-[Re(**diim**)$(CO)_3$(**L**)] (1 eq) was added to dichloromethane and the mixture was allowed to cool down by immersion into an ethyl acetate/liquid nitrogen cold bath. Then, methyl trifluoromethanesulfonate (1.2 eq, solution in dichloromethane) was added. The reaction was stirred under nitrogen for approximately 30 minutes while being kept in the cold bath, then allowed to warm up to room temperature and stirred overnight. Anion exchange was carried out by adding an excess of NH_4PF_6 in water to the solution and stirring for 20 minutes. The product was then extracted using dichloromethane (3 × 15 mL) and the organic components were combined and dried over anhydrous $MgSO_4$. The solvent was

removed *in vacuo* to yield a yellow glassy solid. Each of the complexes showed two distinct systems in the NMR (N1 and N2 linkage isomers) that have been assigned to system 'a' or 'b', where system 'a' has the higher integration ratio. Some of the signals appear as one collapsed broad signal in the ^{13}C spectra and are identified below.

fac-[Re(phen)(CO)$_3$(TphCH$_3$)]$^+$

The complex was purified by reprecipitation from dichloromethane and diethyl ether. Yield 0.064 g (61 %). M.p. 284 ºC (dec.). Elemental analysis for $C_{23}H_{16}F_6N_6O_3PRe \cdot 0.5H_2O$: calculated: C 36.13, H 2.24, N 10.99; found: C 36.03, H 1.86, N 10.85. ν_{max} (ATR)/cm^{-1}: 3095 w, 2032 s (CO, A′(1)), 1911 s (CO, A′(2)), 1897 s (CO, A′′), 1699 w, 1524 w, 1463 w, 1431 w, 1207 w, 1152 w, 832 m, 777 w, 721 w. The ratio of system a:b is 1:0.65. ^1H NMR (δ, ppm, Acetone-d$_6$): 9.73 (2H, d, *J* = 5.2 Hz, phen $H_{2,9}$)^b, 9.30 (2H, d, *J* = 5 Hz, phen $H_{2,9}$)^a, 9.06 (2H, d, *J* = 8.2 Hz, phen $H_{4,7}$)^b, 8.99 (2H, d, *J* = 8.2 Hz, phen $H_{4,7}$)^a, 8.37 (2H, s, phen $H_{5,6}$)^b, 8.33 (2H, s, phen $H_{5,6}$)^a, 8.28-8.24 (2H, m, phen $H_{3,8}$)^b, 8.09-8.06 (2H, m, phen $H_{3,8}$)^a , 7.85-7.80 (2H, m, CN$_4$-C$_6H_5$), 7.68-7.64 (3H, m, CN$_4$-C$_6H_5$), 7.61-7.57 (1H, m, CN$_4$-C$_6H_5$), 7.52-7.42 (4H, m, CN$_4$-C$_6H_5$), 4.08 (3H, s, CH_3)^b, 3.73 (3H, s, CH_3)^a. ^{13}C NMR (δ, ppm, Acetone-d$_6$): 196.3 (*C*O), 196.0 (*C*O), 158.2 (*C*N$_4$-C$_6$H$_5$), 157.4 (*C*N$_4$-C$_6$H$_5$), 155.7, 155.4, 148.1, 147.9, 141.2, 140.9, 133.5, 133.0, 132.0 (collapsed), 130.5 (collapsed), 130.1, 129.6, 128.9 (collapsed), 127.8, 127.6, 122.6, 122.1, 36.9 (*C*H$_3$), 35.6 (*C*H$_3$). Crystals suitable for X-ray analysis (identified as *fac*-[Re(**phen**)(CO)3(**Tph**CH$_3$)]$^+$, $C_{23}H_{16}F_6N_6O_3PRe$) were obtained by liquid-liquid diffusion of diethyl ether into a dichloromthane solution of the complex.

fac-[Re(phen)(CO)$_3$(TbzCH$_3$)]$^+$

The complex was purified by reprecipitation from dichloromethane and diethyl ether. Yield 0.057 g (53 %). M.p. 234 ºC (dec.). Elemental analysis for $C_{24}H_{16}F_6N_6O_4PRe \cdot 0.5H_2O$: calculated: C 36.37, H 2.16, N 10.60; found: C 36.31, H 1.89, N 10.48. ν_{max} (ATR)/cm^{-1}: 3083 (w), 2032 s (CO, A′(1)), 1929 s (CO, A′(2)), 1922 s (CO, A′′), 1699 m, 1548 w, 1520 w, 1430 m, 1310 w, 1206 w, 1179 w,

1146 w, 826 m, 722 w. The ratio of system a:b is 1:0.80.^{1}H NMR (δ, ppm, Acetone-d_6): 10.27 (1H, s, CN_4-C_6H_4-C*H*O)^{a}, 10.09 (1H, s, CN_4-C_6H_4-C*H*O)^{b} , 9.74 (2H, d, *J* = 5.2 Hz, phen $H_{2,9}$)^{b}, 9.34 (2H, d, *J* = 6.25 Hz, phen $H_{2,9}$)^{a}, 9.07 (2H, d, *J* = 8.4 Hz, phen $H_{4,7}$)^{b}, 9.01 (2H, d, *J* = 8.2 Hz, phen $H_{4,7}$)^{a} , 8.38 (2H, s, phen $H_{5,6}$)^{b}, 8.34 (2H, s, phen $H_{5,6}$)^{a}, 8.28-8.25 (2H, m, phen $H_{3,8}$)^{b}, 8.18 (2H, d, *J* = 8.8 Hz, CN_4-C_6H_4-C*H*O H_{meta})^{a}, 8.19-8.08 (2H, m, phen $H_{3,8}$)^{a}, 8.02 (2H, d, *J* = 8.4 Hz, CN_4-C_6H_4-C*H*O H_{meta})^{b}, 7.72-7.69 (4H, m, CN_4-C_6H_4-C*H*O H_{ortho})^{a,b}, 4.13 (3H, s, CH_3)^{b}, 3.77 (3H, s, CH_3)^{a} . ^{13}C NMR (δ, ppm, Acetone-d_6): 196.2 (*C*O), 196.0 (*C*O), 192.6 (*C*HO), 192.4 (*C*HO), 157.6 (*C*N_4-C_6H_4-CHO), 156.8 (*C*N_4-C_6H_4-CHO), 155.8, 155.5, 148.1, 147.9, 141.2, 141.0, 140.1, 139.6, 132.0, 131.6, 131.0, 130.7, 130.5, 129.0 (collapsed), 127.8, 127.7, 127.6, 127.4, 37.1 (*C*H_3), 35.7 (*C*H_3). Crystals suitable for X-ray analysis (identified as *fac*-[Re(**phen**)(CO)3(**Tbz**CH_3)]$^{+}$·$CDCl_3$, $C_{24}H_{16}F_6N_6O_4PRe$·$CDCl_3$) were obtained by vapour diffusion of petroleum spirits (40-60 ºC) into a $CDCl_3$ solution of the complex.

***fac*-[Re(phen)(CO)3(TmebCH$_3$)]$^{+}$**

The complex was purified by reprecipitation from dichloromethane and diethyl ether. Yield: 0.016 g (80 %). M.p.195-197 ºC (dec.). Elemental analysis for $C_{25}H_{18}F_6N_6O_5PRe$·$0.5H_2O$: calculated: C 36.50, H 2.33, N 10.22; found: C 36.66, H 1.96, N 10.10. ν_{max} (ATR)/cm^{-1}: 3099 w, 2031 s (CO, A′(1)), 1931 s (CO, A′(2)), 1917/1897 sh s (CO, A′′), 1713 w, 1637 w, 1604 w, 1524 w, 1465 w, 1433 m, 1286 w, 1207 w, 1150 w, 1120 w, 834 m, 721 w. The ratio of system a:b is 1:0.80. ^{1}H NMR (δ, ppm, Acetone-d_6): 9.74 (2H, d, *J* = 5 Hz, phen $H_{2,9}$)^{b}, 9.35 (2H, d, *J* = 5 Hz, phen $H_{2,9}$)^{a} , 9.07 (2H, d, *J* = 8.2 Hz, phen $H_{4,7}$)^{b}, 9.02 (2H, d, *J* = 8.2 Hz, phen $H_{4,7}$)^{a} , 8.38 (2H, s, phen $H_{5,6}$)^{b}, 8.35 (2H, s, phen $H_{5,6}$)^{a}, 8.28-8.25 (2H, m, phen $H_{3,8}$)^{b}, 8.52 (2H, d, *J* = 8.8 Hz, CN_4-C_6H_4-$COOCH_3$ H_{meta})^{a}, 8.19-8.06 (4H, m, phen $H_{3,8}$ and CN_4-C_6H_4-$COOCH_3$ H_{meta})^{a,b}, 7.62 (4H, d, *J* = 8.6 Hz, CN_4-C_6H_4-$COOCH_3$ H_{ortho})^{a,b},4.12 (3H, s, CH_3)^{b}, 4.03 (3H, s, OCH_3)^{a}, 3.90 (3H, s, OCH_3)^{b}, 3.77 (3H, s, CH_3)^{a}. ^{13}C NMR (δ, ppm, Acetone-d_6): 166.3 (*C*OCH_3), 166.1 (*C*OCH_3), 157.7 (*C*N_4-C_6H_4-$COOCH_3$), 156.8 (*C*N_4-C_6H_4-$COOCH_3$), 155.8, 155.6, 148.1, 148.0, 141.2, 141.0, 134.8,

134.2, 132.01 (collapsed), 131.1 (collapsed), 130.8, 130.0, 129.0 (collapsed), 127.8, 127.7, 126.7, 126.4, 53.1 (O*C*H_3), 52.9 (O*C*H_3), 37.1 (*C*H_3), 35.7 (*C*H_3). Crystals suitable for X-ray analysis (identified as *fac*-[Re(**phen**)(CO)3(**Tmeb**CH_3)]$^+$, $C_{25}H_{18}F_6N_6O_5PRe$) were obtained by liquid-liquid diffusion of petroleum spirits (60-80 ºC) into a dichloromethane solution of the complex.

fac-[Re(bipy)(CO)3(TphCH$_3$)]$^+$

The complex was purified by reprecipitation from dichloromethane and diethyl ether. Yield 0.79 g (79 %). M.p. 230 ºC (dec). Elemental analysis for $C_{21}H_{16}F_6N_6O_3PRe\cdot0.5H_2O$: calculated: C 34.06, H 2.31, N 11.35; found: C 33.84, H 1.97, N 11.12. ν_{max} (ATR)/cm^{-1}: 3127 w, 2031 s (CO, A′(1)), 1931 m (CO,A′(2)), 1898 s (CO, A′′), 1606 w, 1550 w, 1474 w, 1447 w, 1318 w, 1247 w, 1163 w,1111 w, 1074 w, 1027 w, 902 w, 834 s, 768 m, 732 w, 698 w. The ratio of system a:b is 1:0.79. ^{1}H NMR (δ, ppm, Acetone-d$_6$): 9.32 (2H, d, *J* = 5.4 Hz, bipy *H*$_{3,3'}$)^b, 8.93 (2H, d, *J* = 5.2 Hz, bipy *H*$_{3,3'}$)^a, 8.78 (2H, d, *J* = 8.4 Hz, bipy *H*$_{6,6'}$)^b, 8.70 (2H, d, *J* = 8.4 Hz, bipy *H*$_{6,6'}$)^a, 8.46 (2H, t, *J* = 8Hz, bipy *H*$_{5,5'}$)^b, 8.39 (2H, t, *J* = 8Hz, bipy *H*$_{5,5'}$)^a, 7.93-7.90 (2H, m, bipy H$_{4,4'}$)^b, 7.84-7.80 (1H, m, CN$_4$-C$_6$*H*$_5$), 7.75-7.71 (2H, m, bipy *H*$_{4,4'}$)^a, 7.69-7.55 (9H, m, CN$_4$-C$_6$*H*$_5$), 4.22 (3H, s, -C*H*$_3$)b , 3.86 (3H, s, -C*H*$_3$)^a. ^{13}C NMR (δ, ppm, Acetone-d$_6$): 158.5 (*C*N$_4$-C$_6$H$_5$), 157.6 (*C*N$_4$-C$_6$H$_5$), 157.5, 157.3, 155.1, 154.8, 142.1, 141.8, 133.5, 133.1, 130.7, 130.6, 130.2, 129.8, 129.2, 129.0, 125.2, 125.1m 122.7, 122.2, 37.1 (*C*H_3), 35.8 (*C*H_3). Crystals suitable for X-ray analysis (identified as *fac*-[Re(**bipy**)(CO)3(**Tph**CH_3)]$^+$, $C_{21}H_{16}F_6N_6O_3PRe$) were obtained by liquid-liquid diffusion of diethyl ether into a dichloromethane solution of the complex.

fac-[Re(bipy)(CO)$_3$(TbzCH$_3$)]$^+$

The complex was purified by reprecipitation from dichloromethane and diethyl ether. Yield 0.066 g (64 %). M.p. 225 ºC (dec.). Elemental analysis for $C_{22}H_{16}F_6N_6O_4PRe\cdot0.4CHCl_3$: calculated: C 33.32, H 2.05, N 10.41; found: C 36.57, H 1.73, N 10.39 (a corresponding singlet for $CHCl_3$ was observed in the NMR spectrum). ν_{max} (ATR)/cm^{-1}: 3087 w, 2841 w, 2028 s (CO, A′(1)), 1929 s

(CO, A′(2)), 1901 s (CO, A′′), 1706 m, 1606 w, 1554 w, 1473 w, 1447 w, 1314 w, 1202 w, 834 m, 769 m, 731 w. The ratio of system a:b is 1:0.97. ^{1}H NMR (δ, ppm, Acetone-d_6): 10.26 (1H, s, CN_4-C_6H_4-C*H*O)^{b}, 10.13 (1H, s, CN_4-C_6H_4-C*H*O)^{a}, 9.32 (2H, d, *J* = 5.6 Hz, bipy $H_{3,3'}$)^{a}, 8.96 (2H, d, *J* = 5.6 Hz, bipy $H_{3,3'}$)^{b}, 8.78 (2H, d, *J* = 7.6 Hz, bipy $H_{6,6'}$)^{a}, 8.72 (2H, d, *J* = 8.4 Hz, bipy $H_{6,6'}$)^{b}, 8.46 (2H, t, *J* = 8 Hz, bipy $H_{5,5'}$)^{a}, 8.41 (2H, t, *J* = 8 Hz, bipy $H_{5,5'}$)^{b}, 8.21 (2H, d, *J* = 6.4 Hz, CN_4-C_6H_4-CHO H_{meta})^{b}, 8.09 (2H, d, *J* = 6.4 Hz, CN_4-C_6H_4 -CHO H_{meta})^{a}, 7.94-7.90 (2H, m, bipy $H_{4,4'}$)^{a}, 7.88 (4H, d, *J* = 6.8 Hz, CN_4-C_6H_4 -CHO H_{ortho})^{a,b}, 7.77-7.73 (2H, m, bipy $H_{4,4'}$)^{b}, 4.27 (3H, s, CH_3)^{a}, 3.90 (3H, s, CH_3)^{b}. ^{13}C NMR (δ, ppm, Acetone-d_6): 196.3 (*C*O), 196.1 (*C*O), 192.6 (*C*HO), 192.4 (*C*HO), 157.7 (*C*N_4-C_6H_4 -CHO), 157.5, 157.3, 157.0 (*C*N_4-C_6H_4 -CHO), 155.1, 154.9, 142.2, 141.9, 140.2, 139.7, 131.8, 131.0, 130.7 (collapsed), 129.3, 129.1, 127.7, 127.5, 125.2 (collapsed), 37.3 (CH3), 35.9 (CH3). Crystals suitable for X-ray analysis (identified as *fac*-[Re(**bipy**)(CO)3(**Tbz**CH_3)]$^{+}$·$CHCl_3$, $C_{22}H_{16}F_6N_6O_4PRe$·$CHCl_3$) were obtained by vapour diffusion of petroleum spirits (40-60 ºC) into a $CHCl_3$ solution of the complex.

fac-[Re(bipy)(CO)3(TmebCH$_3$)]$^{+}$

The complex was purified by reprecipitation from dichloromethane and diethyl ether. Yield 0.072 g (57 %). M.p. 242-243 ºC. Elemental analysis for $C_{23}H_{18}F_6N_6O_5PRe$: calculated: C 34.99, H 2.30, N 10.64; found: C 35.11 , H 2.38, N 10.45. ν_{max} (ATR)/cm^{-1}: 3091 w, 2952 w, 2030 s (CO, A′(1)), 1908 (1925 sh) s (CO, A′(2)/A′′), 1706 m, 1607 w, 1463 w, 1451 w, 1433 w, 1294 w, 1207 w, 1122 w, 834 m, 775 w, 732 w. The ratio of system a:b is 1:0.92. ^{1}H NMR (δ, ppm, Acetone-d_6): 9.31 (2H, d, *J* = 4.9 Hz, bipy $H_{3,3'}$)^{b}, 8.96 (2H, d, *J* = 5.6 Hz, bipy $H_{3,3'}$)^{a}, 8.77 (2H, d, *J* = 7.8 Hz, bipy $H_{6,6'}$)^{b} , 8.71 (2H, d, *J* = 8 Hz, bipy $H_{6,6'}$)^{a}, 8.48-8.43 (2H, m, bipy $H_{5,5'}$)^{b} , 8.43-8.38 (2H, bipy $H_{5,5'}$)^{a}, 8.26 (2H, d, *J* = 8.2 Hz, CN_4-C_6H_4 -$COOCH_3$ H_{meta})^{a} , 8.14 (2H, d, *J* = 8.8 Hz, CN_4-C_6H_4 -$COOCH_3$ H_{meta})^{b}, 7.93-7.89 (2H, m, bipy $H_{4,4'}$)^{b}, 7.80-7.78 (2H, d, *J* = 8.8 Hz, CN_4-C_6H_4 -$COOCH_3$ H_{ortho})^{a,b}, 7.77-7.73 (2H, m, bipy $H_{4,4'}$)^{a}, 4.25 (3H, s, CH_3)^{b}, 4.01 (3H, s, OCH_3)^{a}, 3.92 (3H, s, OCH_3)^{b}, 3.89 (3H, s, CH_3)^{a}. ^{13}C NMR (δ, ppm, Acetone-d_6): 196.3 (*C*O), 196.1 (*C*O), 166.3

(*C*OCH3), 166.2 (*C*OCH$_3$), 157.8 (*C*N$_4$-C$_6$H$_4$-COOCH$_3$), 157.5, 157.3, 157.0 (*C*N$_4$-C$_6$H$_4$-COOCH$_3$), 155.1, 154.9, 142.1, 141.9, 134.8, 134.2, 131.3, 131.1, 130.8, 130.2, 129.2, 129.0, 126.8, 126.5, 125.2 (collapsed), 53.0 (O*C*H$_3$), 52.9 (O*C*H$_3$), 37.24 (*C*H$_3$), 35.91 (*C*H$_3$). Crystals suitable for X-ray analysis (identified as *fac*-[Re(**bipy**)(CO)3(**Tmeb**CH$_3$)]$^+$, $C_{23}H_{18}F_6N_6O_5PRe$) were obtained by liquid-liquid diffusion of petroleum spirits (60-80 ºC) into a dichloromethane solution of the complex.

X-ray crystallography

Crystal data and collection details for *fac*-[Re(**phen**)(CO)$_3$(**Tph**CH$_3$)][PF$_6$], *fac*-[Re(**bipy**)(CO)$_3$(**Tph**CH$_3$)][CF$_3$SO$_3$]·CH$_2$Cl$_2$, *fac*-[Re(**phen**)(CO)$_3$(**Tbdz**CH$_3$)][PF$_6$]·CDCl$_3$, *fac*-[Re(**bipy**)(CO)$_3$(**Tbdz**CH$_3$)][PF$_6$]·CHCl$_3$, *fac*-[Re(**phen**)(CO)$_3$(**Tmeb**CH$_3$)][PF$_6$] and *fac*-[Re(**bipy**)(CO)$_3$(**Tmeb**CH$_3$)][PF$_6$] are reported in Table 7 and 8. The diffraction experiments were carried out on a Bruker APEX II diffractometer equipped with a CCD detector and using Mo-Kα radiation in the case of *fac*-[Re(**phen**)(CO)$_3$(**Tph**CH$_3$)][PF$_6$] and *fac*-[Re(**bipy**)(CO)$_3$(**Tph**CH$_3$)][CF$_3$SO$_3$]·CH$_2$Cl$_2$,whereas an Oxford Diffraction Gemini diffractometer was employed for *fac*-[Re(**phen**)(CO)$_3$(**Tbdz**CH$_3$)][PF$_6$]·CDCl$_3$, *fac*-[Re(**bipy**)(CO)$_3$(**Tbdz**CH$_3$)][PF$_6$]·CHCl$_3$, *fac*-[Re(**phen**)(CO)$_3$(**Tmeb**CH$_3$)][PF$_6$] and *fac*-[Re(**bipy**)(CO)$_3$(**Tmeb**CH$_3$)][PF$_6$]. Data were corrected for Lorentz polarization and absorption effects (empirical absorption correction SADABS for *fac*-[Re(**phen**)(CO)$_3$(**Tph**CH$_3$)][PF$_6$] and *fac*-[Re(**bipy**)(CO)$_3$(**Tph**CH$_3$)][CF$_3$SO$_3$]·CH$_2$Cl$_2$; analytical numeric absorption correction CrysAlisPro for *fac*-[Re(**phen**)(CO)$_3$(**Tbdz**CH$_3$)][PF$_6$]·CDCl$_3$, *fac*-[Re(**bipy**)(CO)$_3$(**Tbdz**CH$_3$)][PF$_6$]·CHCl$_3$, *fac*-[Re(**phen**)(CO)$_3$(**Tmeb**CH$_3$)][PF$_6$] and *fac*-[Re(**bipy**)(CO)$_3$(**Tmeb**CH$_3$)][PF$_6$]).[32] Structures were solved by direct methods and refined by full-matrix least-squares based on all data using F^2.[33] H-atoms were placed in calculated positions and refined isotropically using a riding model. All non-hydrogen atoms were refined with anisotropic displacement parameters. The crystals of *fac*-[Re(**phen**)(CO)$_3$(**Tph**CH$_3$)][PF$_6$] appear to be pseudo-merohedrally twinned with twin matrix 1 0 0

0 -1 0 0 0 -1 and refined batch factor 0.3378(9). In view of this twinning, similar *U* restraints were applied to the C, O, F and N atoms of *fac*-[Re(**phen**)$(CO)_3$(**Tph**CH_3)][PF_6]. The $[PF_6]^-$ anion of *fac*-[Re(**phen**)$(CO)_3$(**Tbdz**CH_3)][PF_6]·$CDCl_3$ was modelled as being disordered over two sets of sites with site occupancies constrained to 0.5; displacement parameters were restrained to reasonable values. The $CHCl_3$ solvent molecule of *fac*-[Re(**bipy**)$(CO)_3$(**Tbdz**CH_3)][PF_6]·$CHCl_3$ was modelled as being disordered over two sets of sites with occupancies of the two components each constrained to 0.5 after trial refinement. The $[PF_6]^-$ anion of *fac*-[Re(**bipy**)$(CO)_3$(**Tbdz**CH_3)][PF_6]·$CHCl_3$ was also disordered over two sets of sites but with occupancies refined to 0.889(12) and its complement; geometries of the minor component were restrained to ideal values.

Table 7. Structure refinement details for *fac*-[Re(**phen**)$(CO)_3$(**Tph**CH_3)][PF_6] (**1**), *fac*-[Re(**bipy**)$(CO)_3$(**Tph**CH_3)][CF_3SO_3]·CH_2Cl_2 (**2**) and *fac*-[Re(**phen**)$(CO)_3$(**Tbdz**CH_3)][PF_6]·$CDCl_3$ (**3**).

	(**1**)	(**2**)	(**3**)
Formula	$C_{23}H_{16}F_6N_6O_3PRe$	$C_{23}H_{18}Cl_2F_3N_6O_6ReS$	$C_{25}H_{16}Cl_3DF_6N_6O_4PRe$
Fw	755.59	820.59	903.98
T, K	298(2)	100(2)	100(2)
λ, Å	0.71073	0.71073	0.71073
Crystal system	Monoclinic	Monoclinic	Monoclinic
Space Group	$P2_1/c$	$P2_1/n$	$C2/c$
a, Å	12.1607(13)	9.2488(13)	20.7999(12)
b, Å	14.9974(17)	22.212(3)	11.1806(5)
c, Å	14.0496(16)	14.293(2)	26.1866(14)
β, °	90.0710(10)	91.906(2)	99.901(5)
Cell Volume, $Å^3$	2562.3(5)	2934.8(7)	5999.1(5)
Z	4	4	8

D_c, g cm^{-3}	1.959	1.857	2.002
μ, mm^{-1}	4.887	4.461	4.454
F(000)	1456	1592	3488
Crystal size, mm	0.16×0.13×0.11	0.22×0.14×0.12	0.22×0.12×0.03
θ limits, °	1.36–26.00	1.83–25.02	3.63–28.43
Index ranges	-15≤ h ≤ 15 -18≤ k ≤ 18 -17≤ l ≤17	-11≤ h ≤11 -26≤ k ≤ 26 -17≤ l ≤ 17	-23≤ h ≤26 -14≤ k ≤ 14 -34≤ l ≤22
Reflections collected	26732	27401	17010
Independent reflections	5037 [R_{int} = 0.0519]	5166 [R_{int} = 0.0508]	6501 [R_{int} = 0.0965]
Completeness to θ max	99.9%	99.8%	86.1%
Data / restraints / parameters	5037 / 132 / 362	5166 / 0 / 364	6501 / 84 / 479
Goodness on fit on F^2	1.021	1.100	0.938
R_1 (I> 2σ(I))	0.0247	0.0469	0.0548
wR_2 (all data)	0.0539	0.1246	0.0969
Largest diff. peak and hole, e Å^{-3}	0.670 / –0.352	2.991 / –2.729	3.124 / –1.739

Table 8. Structure refinement details for *fac*-[Re(**bipy**)$(CO)_3$(**Tbdz**CH_3)][PF_6]·$CHCl_3$ (**4**), *fac*-[Re(**phen**)$(CO)_3$(**Tmeb**CH_3)][PF_6] (**5**) and *fac*-[Re(**bipy**)$(CO)_3$(**Tmeb**CH_3)][PF_6] (**6**).

	(**4**)	(**5**)	(**6**)
Formula	$C_{23}H_{17}Cl_3F_6N_6O_4PRe$	$C_{25}H_{18}F_6N_6O_5PRe$	$C_{23}H_{18}F_6N_6O_5PRe$
Fw	878.95	813.62	789.6
T, K	100(2)	100(2)	100(2)
λ, Å	0.71073	0.71073	0.71073
Crystal system	Monoclinic	Monoclinic	Monoclinic
Space Group	*C*2/*c*	$P2_1/c$	$P2_1/c$
a, Å	23.0576(9)	18.0672(6)	10.64680(10)
b, Å	16.6963(5)	9.8480(2)	13.10550(10)
c, Å	15.9749(6)	16.8781(6)	19.44800(10)
β, °	97.077(4)	114.201(4)	91.9550(10)
Cell Volume, Å^3	6103.1(4)	2739.12(17)	2712.03(4)
Z	8	4	4
D_c, g cm^{-3}	1.913	1.973	1.934
μ, mm^{-1}	4.375	4.585	4.628
F(000)	3392	1576	1528
Crystal size, mm	0.43×0.19×0.09	0.27×0.23×0.20	0.28×0.24×0.16
θ limits, °	2.88–30.00	3.85–36.45	3.75–45.72
Index ranges	-28≤ h ≤32 -23≤ k ≤23 -22≤ l ≤ 19	-29≤ h ≤29 -16≤ k ≤ 15 -27≤ l ≤27	-21≤ h ≤21 -26≤ k ≤26 -39≤ l ≤39
Reflections collected	38648	81206	181307
Independent	8891 [R_{int} = 0.0763]	12974 [R_{int} = 0.0403]	23179 [R_{int} = 0.0401]

reflections			
Completeness to θ max	99.9%	99.0%	99.8%
Data / restraints / parameters	8891 / 19 / 459	12974 / 0 / 400	23179 / 0 / 381
Goodness on fit on F^2	1.197	0.967	0.874
R_1 ($I > 2\sigma(I)$)	0.0598	0.0360	0.0197
wR_2 (all data)	0.1263	0.0960	0.0400
Largest diff. peak and hole, e $Å^{-3}$	2.474 / –0.96	2.000 / –1.326	1.390 / –0.646

Photophysical measurements

Absorption spectra were recorded at room temperature using a Perkin Elmer Lambda 35 UV/Vis spectrometer. Uncorrected steady state emission and excitation spectra were recorded on an Edinburgh FLSP920 spectrometer equipped with a 450 W Xenon arc lamp, double excitation and single emission monochromators and a Peltier cooled Hamamatsu R928P photomultiplier tube (185-850 nm). Emission and excitation spectra were corrected for source intensity (lamp and grating) and emission spectral response (detector and grating) by a calibration curve supplied with the instrument. The wavelengths for the emission and excitation spectra were determined using the absorption maxima of the metal-to-ligand charge transfer (MLCT) transition bands (emission spectra) and at the maxima of the emission bands (excitation spectra). According to the approach described by Demas and Crosby,[34] luminescence quantum yields (Φ) were measured in optically dilute solutions (O.D. < 0.1 at excitation wavelength) obtained from absorption spectra on a wavelength scale (nm) and compared to the reference emitter by the following equation:

$$F_x = F_r \frac{\left[A_r(\lambda_r)\right]\left[I_r(\lambda_r)\right]\left[n_x^2\right]\left[D_x\right]}{\left[A_x(\lambda_x)\right]\left[I_x(\lambda_x)\right]\left[n_r^2\right]\left[D_r\right]}$$

where *A* is the absorbance at the excitation wavelength (λ), *I* is the intensity of the excitation light at the excitation wavelength (λ), *n* is the refractive index of the solvent, *D* is the integrated intensity of the luminescence and Φ is the quantum yield.[35] The subscripts *r* and *x* refer to the reference and the sample, respectively. The quantum yield determinations were performed at identical excitation wavelengths for the sample and the reference, therefore cancelling the $I(\lambda_r)/I(\lambda_x)$ term in the equation. All the Re(I) complexes were measured against an ethanol solution of Rhodamine 101 used as reference (Φ_r = 1).[36] Emission lifetimes (τ) were determined with the single photon counting technique (TCSPC) with the same Edinburgh FLSP920 spectrometer using pulsed picosecond LEDs (EPLED 295 or EPLED 360, FHWM <800 ps) as the excitation source, with repetition rates between 1KHz and 1 MHz, and the above-mentioned R928P PMT as detector. The goodness of fit was assessed by minimizing the reduced χ^2 function and by visual inspection of the weighted residuals. To record the 77 K luminescence spectra, the samples were put in quartz tubes (2 mm diameter) and inserted in a special quartz dewar filled up with liquid nitrogen. The solvent (dichloromethane) used in the preparation of the solutions for the photophysical investigations were of spectrometric grade. Degassed solutions were prepared by gently bubbling argon gas into the prepared sample for 15 minutes before measurement. Experimental uncertainties are estimated to be ±8% for lifetime determinations, ±20% for quantum yields, ±2 nm and ±5 nm for absorption and emission peaks, respectively.

Photoluminescence in the solid state

The samples in PS matrix were prepared by drop casting of a Re(I) complex:PS blend in dichloromethane solution, with a final film thickness of about 1 mm. Neat films of Re(I) complex

were prepared by thermal-evaporation under vacuum, with a final film thickness of about 200 nm. Solid state absorption and emission measurements were made using a Perkin Elmer Lambda 9 UV/Vis/NIR spectrometer and a Edinburgh FLS920 spectrofluorimeter, respectively. The quantum photoluminescence efficiency was measured with the use of an integrating sphere following Mello's method.[37] The excited state lifetimes of the solid samples were carried out with a single-photon counter IBH model.

Raman and resonance Raman

Fourier-transform Raman (FT-Raman) spectra were obtained from solid samples using a Bruker Equinox-55 FT-interferometer with an FRA106/5 Raman accessory and D418T liquid-nitrogen-cooled Germanium detector. 1064 nm excitation was provided by a Nd:YAG laser. Resonance Raman spectra were recorded using a previously described setup.[38] Solutions were 3 mM in spectroscopic grade dichloromethane. Excitation wavelengths of 350.7, 356.4, 406.7, and 413.1 nm were obtained from a krypton-ion laser (Coherent Innova I-302). Laser power at the sample was about 30 mW. The incident beam and collection lens were arranged in a 135° backscattering geometry to reduce loss of Raman intensity by self-absorption.

Computational calculations

All DFT calculations were performed using Gaussian 09.[39] The SDD effective core potential basis set was used for rhenium and the 6-311G(d,p) basis set was used for all other atoms.[40] The B3LYP functional was used to optimise the rhenium structures in the gas phase and to simulate Raman spectra.[41] Frequencies were scaled by a factor of 0.975 and used to generate simulated spectra as described previously.[38] The mean absolute deviation between experimental and calculated frequencies was less than 10 cm^{-1}. Time-dependent DFT calculations were performed on the gas phase optimized structures using the same method but with PCM solvation in dichloromethane. Electron transition densities were calculated using GaussSum.[42]

OLED device fabrication and characterisation

OLEDs were fabricated by growing a sequence of thin layers on clean glass substrates pre-coated with a layer of indium tin oxide (ITO, 120 nm-thick) with a sheet resistance of 20 Ω per square. A 2 nm-thick hole-injecting layer of MoO_x was deposited on top of the ITO by thermal evaporation under high vacuum of 10^{-6} hPa. All remaining organic layers were deposited in succession by thermal evaporation under high vacuum, followed by thermal evaporation of the cathode layer consisting of 0.5 nm thick LiF and a 100 nm thick aluminium cap. The emitting layer (EML) was evaporated by co-deposition of *fac*-[Re(**phen**)$(CO)_3$(**Tph**)] and TCP in 1:9 mass ratio. The current–voltage characteristics were measured with a Keithley Source-Meter unit, model 236, under continuous operation mode, while the light output power was measured with an EG&G power meter, and electroluminescence (EL) spectra recorded with a StellarNet spectroradiometer. All measurements were carried out at room temperature under an argon atmosphere and were reproduced for many runs.

LEEC device preparation and characterisation

Glass substrates pre-coated with a 120 nm thick layer of ITO with a sheet resistance of 20 Ω per square were patterned by treatment with an acidic solution and cleaned by sonication in acetone and 2-propanol. After drying in a nitrogen flow, the substrates were subsequently kept for 25 minutes in UVO-cleaner (Jetlight Company Model 42-220). The substrates were spin-coated with an aqueous solution of PEDOT (4000 rpm, 60 sec.) and dried in an oven at 140 °C for 10 min. The resulting layer of PEDOT was 40 nm think. Afterwards, 60 nm thick film of a degassed dichloromethane *fac*-[Re(**phen**)$(CO)_3$(**Tph**CH_3)][PF_6] solution with a concentration of 20 mg mL^{-1} was deposited by spin coating (2000 rpm, 1 min). The thickness of the obtained films was measured to with TENCOR Alpha Step I-Q profilometer. The cathode was subsequently deposited by thermal evaporation of aluminium (100 nm) under high vacuum (~10^{-6} hPa) in Edwards Auto 306 evaporator. The mask

used for the evaporation of aluminium cathode framed the circular cell area of 0.071 cm^2. The current-voltage characteristics were measured with a Keithley Source-Measure unit, model 236, under DC mode, while the light output power was measured with an EG&G power meter and electroluminescence (EL) spectra with a StellarNet spectroradiometer. All measurements were carried out at room temperature under argon atmosphere.

Acknowledgments

The work was supported by the Australian Research Council (FT1301000033). MVW wishes to thank Curtin University for an Australian Postgraduate Award. JMM and MC thank Consorzio MIST E-R (project FESR-Tecnopolo AMBIMAT).

Electronic Supplementary Information

X-ray crystal structures for the complexes (CCDC: 1029144-1029149); absorption spectra; emission spectra at RT and 77 K; TD-DFT calculations; Raman and resonance Raman spectra; LEEC performance parameters.

References

1. R. A. Kirgan, B. P. Sullivan, and D. P. Rillema, *Top. Curr. Chem.*, 2007, **281**, 45–100.
2. A. Kumar, S. Sun, and A. Lees, *Top. Organomet. Chem.*, 2010, **29**, 1–35.
3. M. Mauro, E. Procopio, Y. Sun, C. Chien, D. Donghi, M. Panigati, P. Mercandelli, P. Mussini, G. D'Alfonso, and L. De Cola, *Adv. Funct. Mater.*, 2009, **19**, 2607–2614.
4. M. P. Coogan and V. Fernández-Moreira, *Chem. Commun.*, 2013, **50**, 384–399.
5. K. Lo, *Top. Organomet. Chem.*, 2010, **29**, 115–158.
6. C. A. Bader, R. D. Brooks, Y. S. Ng, A. Sorvina, M. V. Werrett, P. J. Wright, A. G. Anwer, D. A. Brooks, S. Stagni, S. Muzzioli, M. Silberstein, B. W. Skelton, E. M. Goldys, S. E. Plush, T. Shandala, and M. Massi, *RSC Adv.*, 2014, **4**, 16345–16351.
7. J. Agarwal, R. P. Johnson, and G. Li, *J Phys Chem A*, 2011, **115**, 2877–2881.
8. T. Morimoto, T. Nakajima, S. Sawa, R. Nakanishi, D. Imori, and O. Ishitani, *J. Am. Chem. Soc.*, 2013, **135**, 16825–16828.
9. A. Vlček, *Top. Organomet. Chem.*, 2010, **29**, 73–114.
10. A. El Nahhas, C. Consani, A. M. Blanco-Rodríguez, K. M. Lancaster, O. Braem, A. Cannizzo, M. Towrie, I. P. Clark, S. Zális, M. Chergui, and A. Vlcek Jr, *Inorg. Chem.*, 2011, **50**, 2932–2943.
11. D. Stufkens and A. Vlček, *Coord. Chem. Rev.*, 1998, **177**, 127–179.
12. E. Kober, J. Caspar, R. Lumpkin, and T. Meyer, *J. Phys. Chem.*, 1986, **90**, 3722–3734.

13. M. V. Werrett, D. Chartrand, J. D. Gale, G. S. Hanan, J. G. MacLellan, M. Massi, S. Muzzioli, P. Raiteri, B. W. Skelton, M. Silberstein, and S. Stagni, *Inorg. Chem.*, 2011, **50**, 1229–1241.
14. M. V. Werrett, S. Muzzioli, P. J. Wright, A. Palazzi, P. Raiteri, S. Zacchini, M. Massi, and S. Stagni, *Inorg. Chem.*, 2014, **53**, 229–243.
15. K. D. M. MaGee, P. J. Wright, S. Muzzioli, C. M. Siedlovskas, P. Raiteri, M. V. Baker, D. H. Brown, S. Stagni, and M. Massi, *Dalton Trans.*, 2013, **42**, 4233–4236.
16. H. Yersin, A. F. Rausch, R. Czerwieniec, T. Hofbeck, and T. Fischer, *Coord. Chem. Rev.*, 2011, **255**, 2622–2652.
17. A. Rausch, H. Homeier, and H. Yersin, *Top. Organomet. Chem.*, 2010, **29**, 193–235.
18. Q. Pei, G. Yu, C. Zhang, Y. Yang, and A. J. Heeger, *Science*, 1995, **269**, 1086–1088.
19. Q. Pei, Y. Yang, G. Yu, C. Zhang, and A. J. Heeger, *J. Am. Chem. Soc.*, 1996, **118**, 3922–3929.
20. D. C. Grills, J. Turner, and M. W. George, *Time-resolved Infrared Spectroscopy*, Comprehensive Coordination Chemistry II, 2003, vol. 2.
21. J. Bredenbeck, J. Helbing, and P. Hamm, *J. Am. Chem. Soc.*, 2004, **126**, 990–991.
22. S. L. Howell and K. C. Gordon, *J. Phys. Chem. A*, 2006, **110**, 4880–4887.
23. R. Butler and V. Garvin, *J. Chem. Soc., Perkin Trans. 1*, 1981, 390–393.
24. A. Palazzi, S. Stagni, S. Bordoni, M. Monari, and S. Selva, *Organometallics*, 2002, **21**, 3774–3781.
25. P. J. Wright, S. Muzzioli, M. V. Werrett, P. Raiteri, B. W. Skelton, D. S. Silvester, S. Stagni, and M. Massi, *Organometallics*, 2012, **31**, 7566–7578.
26. M. Itokazu, A. Polo, and N. Iha, *J. Photochem. Photobiol. A*, 2003, **160**, 27–32.
27. M. A. Baldo, S. Lamansky, P. E. Burrows, M. E. Thompson, and S. R. Forrest, *Appl. Phys. Lett.*, 1999, **75**, 4–6.
28. J. Kalinowski, W. Stampor, M. Cocchi, D. Virgili, V. Fattori, and P. Di Marco, *Chem Phys*, 2004, **297**, 39–48.
29. P. Brulatti, R. J. Gildea, J. A. K. Howard, V. Fattori, M. Cocchi, and J. A. G. Williams, *Inorg. Chem.*, 2012, **51**, 3813–3826.
30. J. Li, Z. Si, C. Liu, C. Li, F. Zhao, Y. Duan, P. Chen, S. Liu, and B. Li, *Semicond. Sci. Technol.*, 2007, **22**, 553–556.
31. R. D. Costa, E. Ortí, H. J. Bolink, F. Monti, G. Accorsi, and N. Armaroli, *Angew. Chem. Int. Ed.*, 2012, **51**, 8178–8211.
32. R. C. Clark and J. S. Reid, *Acta Cryst. A*, 1995, **51**, 887–897.
33. G. M. Sheldrick, *Acta Cryst. A*, 2008, **64**, 112–122.
34. J. Demas and G. Crosby, *J. Phys. Chem.*, 1971, **75**, 991–1024.
35. D. Eaton, *Pure Appl. Chem.*, 1988, **60**, 1107–1114.
36. T. Karstens and K. Kobs, *J. Phys. Chem.*, 1980, **84**, 1871–1872.
37. J. C. de Mello, H. F. Wittmann, and R. H. Friend, *Adv. Mater.*, 2004, **9**, 230–232.
38. R. Horvath, M. G. Fraser, S. A. Cameron, A. G. Blackman, P. Wagner, D. L. Officer, and K. C. Gordon, *Inorg. Chem.*, 2013, **52**, 1304–1317.
39. M. J. Frisch, G. W. Trucks, H. B. Schlegel, G. E. Scuseria, M. A. Robb, J. R. Cheeseman, G. Scalmani, V. Barone, B. Mennucci, G. A. Petersson, H. Nakatsuji, M. Caricato, X. Li, H. P. Hratchian, A. F. Izmaylov, J. Bloino, G. Zheng, J. L. Sonnenberg, M. Hada, M. Ehara, K. Toyota, R. Fukuda, J. Hasegawa, M. Ishida, T. Nakajima, Y. Honda, O. Kitao, H. Nakai, T. Vreven, J. A. Montgomery, Jr, J. E. Peralta, F. Ogliaro, M. Bearpark, J. J. Heyd, E. Brothers, K. N. Kudin, V. N. Staroverov, R. Kobayashi, J. Normand, K. Raghavachari, A. Rendell, J. C. Burant, S. S. Iyengar, J. Tomasi, M. Cossi, N. Rega, J. M. Millam, M. Klene, J. E. Knox, J. B. Cross, V. Bakken, C. Adamo, J. Jaramillo, R. Gomperts, R. E. Stratmann, O. Yazyev, A. J. Austin, R. Cammi, C. Pomelli, J. W. Ochterski, R. L. Martin, K. Morokuma, V. G. Zakrzewski, G. A. Voth, P. Salvador, J. J. Dannenberg, S. Dapprich, A. D. Daniels, Ö.

Farkas, J. B. Foresman, J. V. Ortiz, J. Cioslowski, and D. J. Fox, Gaussian 09, Revision A.02.
40. D. Andrae, U. Haeussermann, M. Dolg, H. Stoll, and H. Preuss, *Theor. Chim. Acta*, 1990, **77**, 123–141.
41. A. D. Becke, *J. Chem. Phys.*, 1993, **98**, 5648–5652.
42. N. M. O'boyle, A. L. Tenderholt, and K. M. Langner, *J. Comput. Chem.*, 2008, **29**, 839–845.